Available online at www.sciencedirect.com
ScienceDirect
Journal of Virological Methods 143 (2007) 95–103
Journal of Virological Methods
www.elsevier.com/locate/jviromet

Optimization of the virus concentration method using polyethyleneimine-conjugated magnetic beads and its application to the detection of human hepatitis A, B and C viruses

Eriko Uchida [a], Mieko Kogi [a,b], Tadashi Oshizawa [a], Birei Furuta [a], Koei Satoh [c], Akiko Iwata [c], Mitsuhiro Murata [d], Mikio Hikata [d], Teruhide Yamaguchi [a,e,*]

[a] *Division of Cellular and Gene Therapy Products, National Institute of Health Sciences, 1-18-1 Kamiyoga, Setagaya, Tokyo 158-8501, Japan*
[b] *Kanazawa Institute of Technology, Nonoichi, Ishikawa, Japan*
[c] *The Institute of the Saitama Red Cross Center, Kumagaya, Saitama, Japan*
[d] *JSR Corporation, Tsukuba Research Laboratories, Tsukuba, Ibaraki, Japan*
[e] *Division of Biological Chemistry and Biologicals, National Institute of Health Sciences, 1-18-1 Kamiyoga, Setagaya, Tokyo 158-8501, Japan*

Received 25 September 2006; received in revised form 22 February 2007; accepted 26 February 2007
Available online 12 April 2007

Abstract

To enhance the sensitivity of virus detection by polymerase chain reaction (PCR) and reverse transcription PCR (RT-PCR), a novel virus concentration method using polyethyleneimine (PEI)-conjugated magnetic beads was developed in our previous study. However, several viruses could not be concentrated by this method. In this paper, the conditions of virus concentration were optimized to concentrate a wide range of viruses more efficiently. The PEI beads adsorbed viruses more efficiently than other cationic polymers, and the optimum virus concentration was obtained under weak acidic conditions. Mass spectrometric analysis revealed that several serum proteins, such as complement type 3, complement type 4 and immunoglobulin M (IgM), were co-adsorbed by the PEI beads, suggesting that the beads may adsorb viruses not only by direct adsorption, but also via immune complex formation. This hypothesis was confirmed by the result that poliovirus, which PEI beads could not adsorb directly, could be concentrated by the beads via immune complex formation. On the other hand, hepatitis A (HAV) and hepatitis C (HCV) viruses were adsorbed directly by PEI beads almost completely. Like poliovirus, hepatitis B virus (HBV) was concentrated efficiently by the addition of anti-HBV IgM. In conclusion, virus concentration using PEI beads is a useful method to concentrate a wide range of viruses and can be used to enhance the sensitivity of detection of HAV, HBV and HCV.

Keywords: Polyethyleneimine; Virus concentration; Immune complex; HAV; HBV; HCV

1. Introduction

Many useful biological/biotechnological medicinal products are produced from biological materials and by cell culture techniques. Recent progress in gene therapy and cell therapy products has provided new hope for the treatment of grave genetic diseases and lethal disorders. These innovative medicinal products, however, involve some risk in terms of the spread of transmissible agents and virus-mediated infectious diseases. To ensure the viral safety of biological/biotechnological products, it is important to confirm that the starting materials, intermediate products and final products are free from virus contamination. This is especially important for cell therapy products, since it is difficult to inactivate and/or remove contaminated viruses from these products.

Polymerase chain reaction (PCR) is a highly sensitive method for the detection of virus genomes (Saiki et al., 1988). Several nucleic acid amplification test (NAT) methods other than PCR have also been developed (Alter et al., 1995; Kamisango et al., 1999; Kern et al., 1996; Notomi et al., 2000; Sarrazin et al., 2000). These tests are reported to be able to detect only some copies of virus genomes. Therefore, in many countries, NAT methods have been employed to detect specific viruses in the virus screening of blood-derived products (Willkommen et al.,

* Corresponding author. Tel.: +81 3 3700 9064; fax: +81 3 3700 9084.
E-mail address: yamaguch@nihs.go.jp (T. Yamaguchi).

0166-0934/$ – see front matter © 2007 Elsevier B.V. All rights reserved.
doi:10.1016/j.jviromet.2007.02.014

1999). NAT methods are also thought to be useful in testing biotechnology products derived from cell lines and cell therapy products. However, since all NAT methods used for the detection of viruses have a detection limit, it is impossible to deny virus contamination completely. In order to reduce the virus risk of both biological/biotechnological products and cell therapy products, it is essential to develop more sensitive methods of virus detection. One way to improve the sensitivity of virus detection is to concentrate the target viruses before NAT testing.

Recently, a novel viral concentration method using polyethyleneimine (PEI)-conjugated magnetic beads was developed (Satoh et al., 2003). It was shown that PEI beads efficiently adsorbed many model viruses, such as simian virus 40 (SV-40), herpes simplex 1 virus (HSV-1), Sindbis virus and vesicular stomatitis virus (VSV), and that the method improved the sensitivity of NAT for the detection of virus genomes about 10 to 100 times. It has also been reported that PEI beads efficiently adsorb amphotropic murine leukemia virus, and that the virus concentration method provided sensitive detection of replication-competent retrovirus in retrovirus vector products (Uchida et al., 2004). However, several small non-enveloped viruses such as poliovirus could not be concentrated or were only partially concentrated by PEI beads (Satoh et al., 2003). In addition, the mechanism of virus adsorption by PEI beads remains to be elucidated.

In the present study, the viral concentration method using PEI beads was optimized in order to allow the efficient concentration of several viruses. It was demonstrated that poliovirus can be concentrated by PEI beads via the formation of immune complexes. In addition, it was shown that the virus concentration method using PEI beads is applicable to human infectious viruses such as the hepatitis A(HAV), hepatitis B (HBV) and hepatitis C (HCV) viruses, which are important viruses to test for in order to ensure the viral safety of biological products and cell therapy products.

2. Materials and methods

2.1. Viruses

SV-40 virus, HSV-1 (stain F), porcine parvovirus (PPV; strain 90HS) and poliovirus (strain Sabin 1) were obtained and amplified as described previously (Satoh et al., 2003). Briefly, the supernatants of Vero cells infected with HSV-1 or poliovirus were used as virus samples. CV-1 cells were infected with SV-40 virus, and 5 days after infection, the supernatant was saved as the SV-40 sample. The supernatant of ESK cells infected with PPV was used as the PPV sample. In order to remove cell debris from the collected virus suspension, each virus suspension was centrifuged at 3000 rpm for 10 min. After removing cell debris, the resulting stock viruses (SV40: 4×10^7 copies/ml; PPV: 1×10^6 copies/ml; HSV-1: 1×10^8 copies/ml; poliovirus: 2×10^7 copies/ml) were aliquoted and stored at −80 °C until use. Human adenovirus type 5 reference material (ATCC VR-1516; 5.8×10^{11} particles/ml) was obtained from the American type culture collection (ATCC) and used without amplification. HAV was obtained from ATCC (strain HM175/18f), infected into FRhK-4 cells, and the supernatant of the cell was saved 9–11 days later as the HAV sample (1×10^8 PFU/ml). The first Japanese national standard for HBV DNA (Genotype C; potency: 4.4×10^5 IU/ml) and the first Japanese national standard for HCV RNA (Mizusawa et al., 2005); genotype HCV-1b; potency: 100,000 IU/ml) were directly used as the HBV sample and HCV sample, respectively.

2.2. Preparation of PEI beads

PEI beads were prepared by coupling PEI (MW 70,000; Wako Pure Chemical Industries, Ltd., Tokyo, Japan) with magnetic beads (IMMUTEX-MAG™; mean diameter: 0.8 μm; JSR Inc., Tokyo, Japan) by the 1-ethylene-3-(3-dimethylaminopropyl) carbodiimide coupling method, as described previously (Satoh et al., 2003). The final concentration of the PEI beads was 50 mg/ml. Different molecular weights of PEI beads were prepared as described above but including the coupling of PEI with a molecular weight (MW) of 1800 or PEI (MW 10,000) to magnetic beads, instead of PEI (MW 70,000). Polyarylamine (PAA)-conjugated magnetic beads and poly-L-lysine (PLL)-conjugated magnetic beads were prepared in the same way as PEI beads, using PAA (MW 150,000) or PLL (MW > 300,000) instead of PEI, respectively.

2.3. Virus concentration using PEI beads

The essential adsorption procedure for each virus was as follows. Virus samples were diluted with virus dilution medium (Dulbecco's modified Eagle's medium (DMEM) or DMEM supplemented with 2% fetal calf serum (FCS)). The exact concentration of the virus suspension used for each experiment is described in the corresponding figure legends. Next, 1 ml of each virus suspension was incubated with 100 μl of PEI beads for 10 min at room temperature. The complexes of virus and PEI beads were trapped by a magnetic field (Magnetic Trapper™; Toyobo Co., Tokyo, Japan) for 5 min and separated from the supernatant fraction. The virus DNA or RNA was extracted from virus-bead complex or from untreated virus suspensions (100 μl) with an SMI-TEST EX R&D Kit (Medical & Biological Laboratories Co., Nagano, Japan) following the manufacturer's instructions. Extracted DNA or RNA was dissolved in 50 μl of TE buffer (10 mM Tris–HCl (pH 7.4)/0.1 mM EDTA), and 10 μl of the solution was used for real-time PCR or RT-PCR reaction.

2.4. Effect of pH on virus concentration by PEI beads

Good's buffers with pH 4–9 (1 M MES, pH 4.0; 1 M MES, pH 5.0; 1 M MES, pH 6.0; 1 M HEPES, pH 7.0; 1 M HEPES, pH 8.0; 1 M Tricine, pH 9.0) were prepared and added to the virus dilution medium at a final concentration of 20 mM. Virus samples were then diluted with the virus dilution media at different pH values, and concentrated with PEI beads as described. The exact concentration of the virus suspension used for each experiment is described in the corresponding figure legends.

2.5. Real-time PCR and RT-PCR

Real-time PCR and reverse transcription PCR (RT-PCR) were carried out in a 50-μl reaction mixture containing 10 μl of extracted DNA or RNA, 0.5 μM of each primer set with a fluorescence probe, 25 μl of PCR master mix and, in the case of RT-PCR, a reverse transcriptase mix prepared according to the kit manual. The following real-time PCR and RT-PCR master mix kits were used: a QuantiTect Probe PCR kit (Qiagen, Hilden, Germany) for HSV-1, SV-40, adenovirus and PPV; a QuantiTect Probe RT-PCR kit (Qiagen) for poliovirus, HAV and HCV; and a Platinum Quantitative PCR SuperMix-UDG with ROX (Invitrogen, Carlsbad, CA, USA) for HBV. The 5′-primers, 3′-primers and fluorescence probes used for the real-time PCR and RT-PCR detection of viruses are shown in Table 1. The real-time PCR and RT-PCR were performed on an ABI PRISM 7000 Sequence-Detection System (Applied Biosystems, Foster City, CA, USA).

2.6. SDS-PAGE analysis of serum proteins adsorbed on PEI beads

The virus suspension (HSV-1) diluted with DMEM supplemented with 5% FCS was incubated with PEI beads for 10 min. The fraction of serum proteins adsorbed on the beads and the untreated virus suspension were then boiled with sodium dodecly sulfate (SDS) sample buffer and applied to SDS-polyacrylamide gel electrophoresis (SDS-PAGE). SDS-PAGE was carried out on a slab gel ($T = 7.5\%$) with a BE-120 system from Biocraft (Tokyo, Japan). Protein bands were visualized by Coomassie Brilliant Blue staining.

2.7. In-gel digestion

Protein bands of interest were excised from the SDS-PAGE gel, destained three times in 50% acetonitrile and 25 mM ammonium bicarbonate for 10 min each time, and dehydrated in acetonitrile. The gel pieces were dried in a vacuum centrifugal concentrator and incubated with 10 mM dithiothreitol (DTT) in 25 mM ammonium bicarbonate at 56 °C for 60 min. After cooling to room temperature, the DTT solution was replaced with roughly the same volume of 55 mM iodoacetamide in 25 mM ammonium bicarbonate. After incubation for 45 min at room temperature in the dark, the gel pieces were washed in 25 mM ammonium bicarbonate for 5 min and dehydrated by the addition of 50% acetonitrile and 25 mM ammonium bicarbonate for 5 min. After this procedure was repeated twice, the gel pieces were dried in a centrifugal concentrator. The gel pieces were allowed to swell in 2 μl of a digestion buffer containing 25 mM ammonium bicarbonate, 0.1% octyl glucoside, and 25 ng/μl trypsin (sequence grade; Promega, Madison, WI, USA) in ice for 5 min, and then 15 μl of a digestion buffer without trypsin was added. After 30 min, the supernatant was discarded, and the gel pieces were incu-

Table 1
Primer and probe sets used for the real-time PCR and RT-PCR

Virus	Primer and probe set
HSV-1	Forward primer: 5′-GCGTCATGGTACTGGCAAG-3′ Reverse primer: 5′-TTGACTCTACGGAGCTGGCC-3′ Probe: 5′-FAM-TGGAGCTGATGCCGTAGTCGG-TAMRA-3′
SV-40	Forward primer: 5′-GACATTCCTAGGCTCACCTCACA-3′ Reverse primer: 5′-ACCTTGCCAAACTGTCCCTTAAA-3′ Probe: 5′-FAM-CTTGAAAGAAGAACCCAAAGA-TAMRA-3′
PPV	Forward primer: AACAACTACGCAGCAACTCCAATA-3′ Reverse primer: ACGGCTCCAAGGCTAAAGC-3′ Probe: 5′-FAM-AGGAGGACCTGGATTT-MGB-3′
Adenovirus[*1]	Forward primer: TCCGGTCCTTCTAACACACCTC-3′ Reverse primer: ACGGCAACTGGTTTAATGGG-3′ Probe: 5′-FAM-TGAGATACACCCGGTGGTCCCGC-TAMRA-3′
Poliovirus	Forward primer: 5′-CCCGAGAAATGGGACGACTA-3′ Reverse primer: 5′-TGGAGCTGTTCCGTAGGTGTAA-3′ Probe: 5′- FAM-ACATGGCAAACCTCATCAAATCCATCAATC-MGB-3′
HAV[*2]	Forward primer: 5′-GGTAGGCTACGGGTGAAAC-3′ Reverse primer: 5′-AACAACTCACCAATATCCGC-3′ Probe: 5′-FAM-CTTAGGCTAATACTTCTATGAAGAGATGC-TAMRA-3′
HBV[*3]	Forward primer: 5′-GGACCCCTGCTCGTGTTACA-3′ Reverse primer: 5′-GAGAGAAGTCCACCMCGAGTCTAGA-3′ Probe: 5′-FAM-TGTTGACAARAATCCTCACCATACCRCAGA-TAMRA-3′
HCV[*4]	Forward primer: 5′-TGCGGAACCGGTGAGTACA-3′ Reverse primer: 5′-CTTAAGGTTTAGGATTCGTGCTCAT-3′ probe: 5′-FAM-CACCCTATCAGGCAGTACCACAAGGCC-TAMRA-3′

Each primer set was prepared according to the original papers described below ([*1] to [*4]) or designed using Primer Express software (Applied Biosystems). [*1] Adenovirus (Ishii-Watabe et al., 2003), [*2] HAV (Jothikumar et al., 2005), [*3] HBV (Pas et al., 2000), [*4] HCV (Martell et al., 1999).

bated overnight at 37 °C. To extract tryptic fragments, the gel pieces were shaken in 50% acetonitrile and 5% trifluoroacetic acid (TFA) for 30 min. After this procedure was repeated twice, the extraction solutions were pooled, dried in a centrifugal evaporator, and dissolved in 20 μl of 0.1% TFA. The samples were then absorbed onto reverse-phase ZipTipC18 (Millipore, Bedford, MA, USA). The resin was washed with 0.1% TFA and the peptides were eluted with 3 μl of 75% acetonitrile/0.1% TFA. The eluate was analyzed by mass spectrometry (MS) as described below.

2.8. MS and database searching

The peptide mixture (0.5 μl volume) elution was deposited onto a matrix assisted laser desorption/ionization (MALDI) target plate, and this was closely followed by the deposition of 0.5 μl of a saturated solution of α-cyano-4-hydroxycinnamic acid in 50% acetonitrile containing 0.1% TFA. MS and tandem MS (MS/MS) analysis of the peptide mixtures was performed using a 4700 Proteomics Analyzer (Applied Biosystems, Framingham, MA, USA). Peptide mass fingerprinting and MS/MS ion searches were performed for protein identification by a Mascot search based on the MSDB protein database.

2.9. Preparation of anti-mouse IgG-rabbit IgM antibody

Anti-mouse immunogloblulin G (IgG) rabbit antiserum was obtained from rabbits immunized with highly purified mouse IgG (11 mg/ml; Jackson ImmunoResearch, West Grove, PA, USA) at 11 days after immunization, when IgM titer was increased. The antiserum (3 ml) was then diluted with an equal volume of phosphate buffered saline (PBS) (−), and applied to a mouse-IgG agarose affinity column (Invitrogen). After washing with 10 ml of PBS (−), the bound fraction was eluted with 0.1 M glycine–HCl (pH 3.0) and neutralized with 1 M Tris–HCl (pH 8.0). A PEI-sepharose-6MB column was prepared by coupling PEI to CNBr-activated sepharose-6MB (GE Healthcare Bioscience, Piscataway, NJ, USA). Anti-mouse IgG rabbit antiserum purified with a mouse IgG-agarose column was applied to a PEI-sepharose-6MB column and washed with PBS (−), and the bound fraction was eluted with 1.4 M NaCl/50 mM HEPES (pH 7.6). The eluted fraction was concentrated and used as anti-mouse IgG rabbit IgM antibody (final concentration, 4 μg/ml).

2.10. Poliovirus concentration via immune complexes

When poliovirus suspension was concentrated by PEI beads via immune complex formation, anti-poliovirus 1 mouse monoclonal antibody (IgG1: 5 μl; Chemicon International, Temecula, CA, USA) and purified anti-mouse IgG rabbit IgM antibody (20 μl), or anti-poliovirus 1 mouse monoclonal antibody and human complement C1 (5 μl; Merck Biosciences/Calbiochem, Darmstadt, Germany) and C4 (3 μl; Calbiochem) were added to the virus suspension before incubation with PEI beads.

2.11. Preparation of anti-HBV IgM antibody

Anti-hepatitis B surface antigen (HBsAg) IgM antibody was prepared as follows. Rabbits were immunized with a mixture of the adw and adr subtypes of recombinant HBsAg (Advanced ImmunoChemical, Long Beach, CA, USA). Anti-HBsAg rabbit antiserum was obtained at 10 days after immunization, when IgM titer was increased. The antiserum (3 ml) was diluted with an equal volume of PBS (−), applied to a PEI-sepharose-6MB column, washed with 20 ml PBS (−), and eluted with 1.4 M NaCl/100 mM HEPES (pH 7.0). PEI-sepharose-6MB-bound fractions were pooled, desalted with a PD-10 column equilibrated with 1.2 M NaCl/50 mM HEPES buffer (pH 7.4), and purified with an ImmunoPure IgM purification kit (Pierce Biotechnology, Rockford, IL, USA). IgM fractions were concentrated and used as anti-HBsAg IgM antibody.

3. Results

3.1. Optimization of the virus concentration method using PEI beads

In order to optimize the virus concentration method using PEI beads, the relationship between the MW of PEI coupled with magnetic beads and the efficiency of the virus concentration was examined. When PEIs with average molecular masses of 1800, 10,000 and 70,000 Da were compared, the PEI of MW 70,000 Da efficiently concentrated HSV-1, while magnetic beads with the PEI of MWs 1800 and 10,000 Da could not adsorb HSV-1 (Fig. 1). Therefore, the PEI beads with MW 70,000 Da were used in the following experiments.

Next, the virus adsorption ability of PEI was compared to that of other cationic polymers. As shown in Fig. 2, PEI beads exhibited a markedly higher virus adsorption ability than PAA- or PLL-conjugated magnetic beads for all model viruses tested.

The effect of pH on the efficiency of virus concentration was then examined. HSV-1 and SV-40 virus suspensions at different

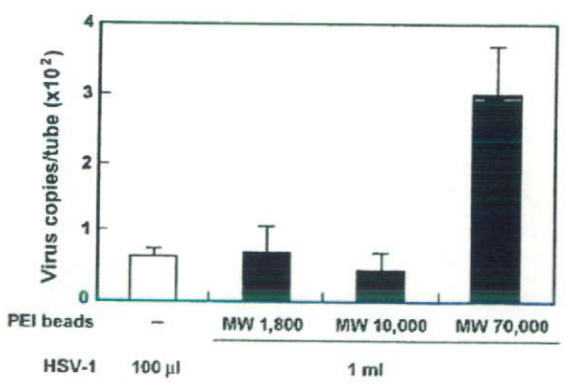

Fig. 1. Comparison of virus concentrations by magnetic beads coupled with PEIs of three different molecular weights. HSV-1 suspension (1×10^3 copies/ml, 1 ml/tube) was incubated with PEI beads whose PEI had a molecular weight of 1800, 10,000 or 70,000 Da. Viral genome DNA was extracted from the PEI bead fraction and from untreated HSV-1 suspension (100 μl). Virus copy numbers were determined by real-time PCR. Data are expressed as the mean ± S.D. ($n = 3$).

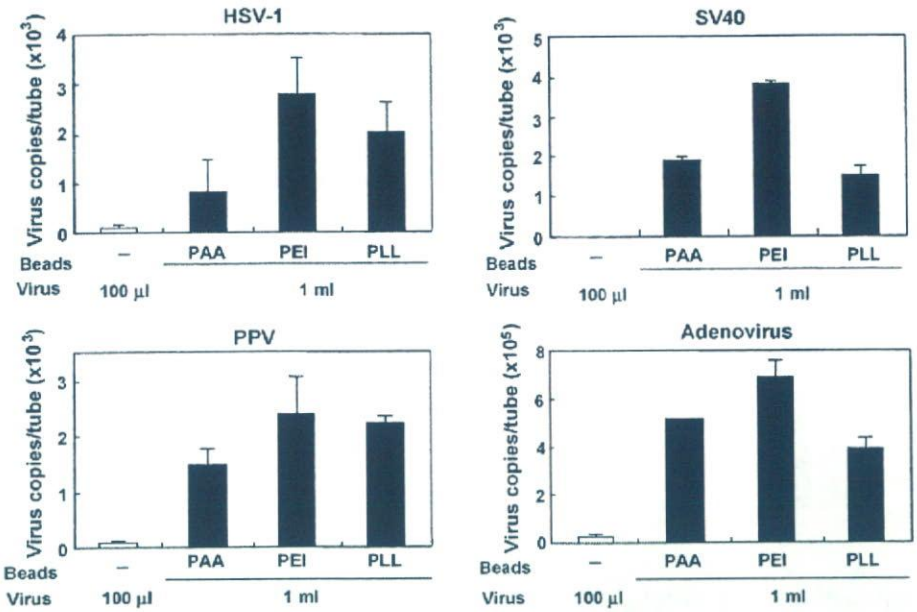

Fig. 2. Comparison of virus concentration by magnetic beads coupled with three different cationic polymers. HSV-1 (5×10^3 copies/ml), SV-40 (5×10^3 copies/ml), PPV (5×10^3 copies/ml) and adenovirus suspensions (1×10^6 copies/ml) (1 ml each) were incubated with PAA-, PEI- or PLL-conjugated magnetic beads. Viral genome DNA was extracted from each magnetic bead fraction and from untreated virus suspensions (100 µl each). Virus copy numbers were determined by real-time PCR. Data are expressed as the mean ± S.D. ($n = 3$).

pH levels (pH 5–9) were concentrated by PEI beads following the standard method. A pH levels of 6 was found to be optimal for the concentration of these viruses (Fig. 3).

3.2. Analysis of serum proteins adsorbed on PEI beads

To improve the virus concentration method using PEI beads, the serum components co-adsorbed by the beads during virus concentration were analyzed. When a virus suspension containing 5% FCS was concentrated by PEI beads and analyzed by SDS-PAGE, several proteins were specifically adsorbed by the beads (Fig. 4). Using MS and MS/MS analyses of these protein bands, complement type 3, complement type 4 and IgM heavy chain were identified as serum components concentrated by PEI beads. Since complement components and IgM were adsorbed by the beads, it is hypothesized that PEI beads may adsorb viruses not only by direct adsorption, but also via the formation of immune complexes that involve IgM antibody and/or complements.

3.3. Concentration of poliovirus by PEI beads via immune complexes

To confirm this hypothesis, concentrations of poliovirus, which PEI beads could not adsorb directly, via the formation of immune complexes were examined. Instead of anti-poliovirus IgM antibody, anti-poliovirus mouse monoclonal antibody (IgG) was used in combination with anti-mouse IgG rabbit IgM anti-

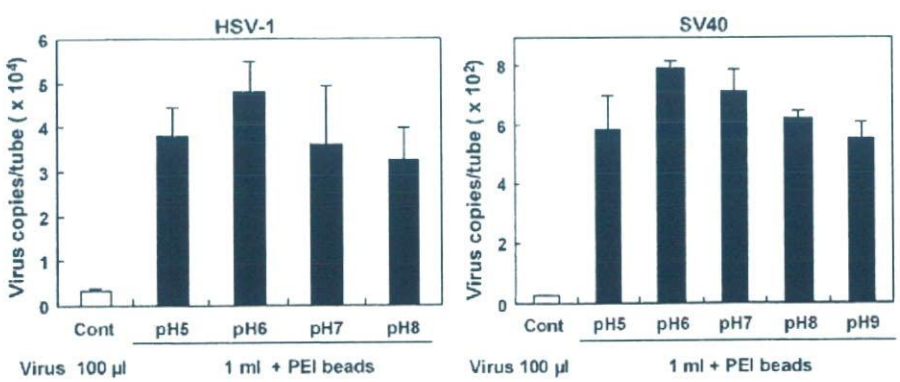

Fig. 3. Effect of pH on the efficiency of virus concentration by PEI beads. HSV-1 (5×10^4 copies/ml) and SV-40 (1×10^3 copies/ml) suspensions diluted with virus dilution medium at different pH levels (HSV-1: pH 5, 6, 7 and 8; SV-40: pH 5, 6, 7, 8 and 9) (1 ml each) were incubated with PEI beads. Viral genome DNA was then extracted from PEI bead fraction and from untreated virus suspensions (100 µl each). Virus copy numbers were determined by real-time PCR. Data are expressed as the mean ± S.D. ($n = 3$).

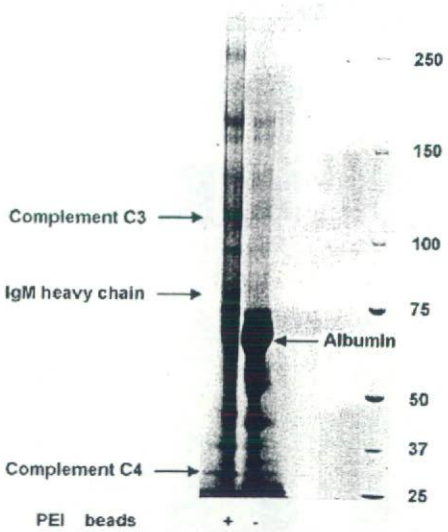

Fig. 4. Serum proteins adsorbed on PEI beads during virus concentration. HSV-1 suspension diluted with DMEM supplemented with 5% FCS was incubated with PEI beads. PEI bead fraction (+) and untreated virus suspension (−) were then boiled with SDS sample buffer and applied to SDS-PAGE. Serum protein bands concentrated by PEI beads were identified by MS/MS analysis, as shown in Fig. 5.

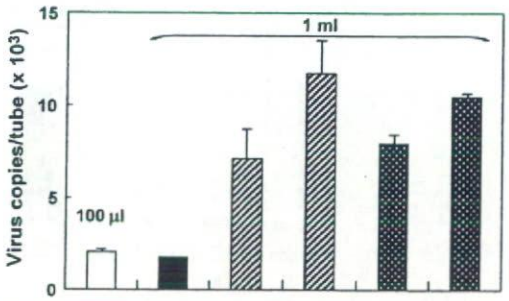

PEI beads	-	+	+	+	+	+
Anti-poliovirus mouse IgG MoAb	-	-	+	+	+	+
Anti-mouse IgG-rabbit IgM	-	-	-	+	-	-
C1 + C4	-	-	-	-	+ (r.t.)	+ (37°C)

Fig. 6. Concentration of poliovirus by PEI beads via the formation of immune complexes. Poliovirus suspension (2×10^4 copies/ml, 1 ml each) was incubated with PEI beads at room temperature or 37 °C in the absence or presence of anti-poliovirus mouse IgG monoclonal antibody, anti-mouse IgG-rabbit IgM, or a combination of complements C1 and C4. Viral genome RNA was extracted from the PEI bead fraction and from the untreated virus suspension (100 µl). Virus copy numbers were determined by real-time RT-PCR. Data are expressed as the mean ± S.D. ($n = 3$).

body to induce the formation of immune complexes. Anti-mouse IgG rabbit IgM antibody was prepared from rabbit anti-mouse IgG antiserum and purified by a mouse-IgG affinity column followed by a PEI-sepharose-6MB column. Since the PEI-sepharose-6MB column adsorbed IgM (Fig. 5) but not IgG (data not shown), the PEI-sepharose-6MB adsorbed fraction was used as the anti-mouse IgG rabbit IgM antibody. When poliovirus alone was incubated with the PEI beads, it was not adsorbed, but poliovirus was adsorbed when coincubated with anti-poliovirus IgG antibody, and a further significant improvement in the efficiency of virus concentration was achieved by the addition of anti-mouse IgG rabbit IgM along with the anti-poliovirus IgG (Fig. 6). The addition of the combination of complement C1, complement C4 and anti-poliovirus IgG to the reaction mixture of virus and PEI beads also increased the efficiency of virus concentration by PEI beads, but only when the complement system was activated by [incubation at] 37 °C (Fig. 6).

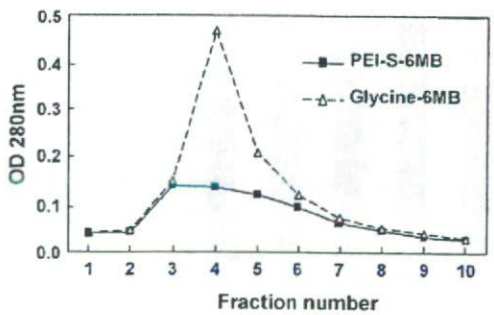

Fig. 5. Adsorption of IgM to a PEI-sepharose column. One ml of human IgM solution (1 mg/ml) was applied to a PEI-sepharose 6MB (PEI-S-6MB) column or to a control column without PEI (Glycine-6 MB) and washed with PBS (−). The eluates were fractionated into ten 1 ml fractions, and the OD280 of each fraction was determined using a spectrophotometer.

3.4. Application of the virus concentration method using PEI beads to human hepatitis viruses

The virus concentration method using PEI beads was applied to human HAV, HBV and HCV. Fig. 7 shows the effect of pH on the virus concentration efficiency. HAV was efficiently adsorbed by the PEI beads (Fig. 7A). The number of viral copies obtained in the PEI bead fraction when using 1 ml of virus suspension was about 10-fold the number extracted from untreated virus suspension (100 µl), suggesting that the concentration of HAV almost reached the predicted level. Neither the presence or absence of serum nor the pH condition affected the efficiency of the HAV concentration. HCV was also efficiently adsorbed by PEI beads, even in the presence of 2% FCS, and the optimum pH was found to be 5 (Fig. 7C). On the other hand, the efficiency of HBV concentration by PEI beads was lower than the efficiencies of HAV and HCV concentrations. The number of viral copies obtained in the PEI bead fraction under the optimum condition of pH 5 without serum was about six-fold the number extracted from untreated virus suspension (Fig. 7B). The presence of FCS significantly reduced the adsorption of HBV by PEI beads.

In order to improve the concentration of HBV obtained by PEI beads, anti-HBV IgM antibody was prepared and the concentration of HBV via immune complex formation was examined. As shown in Fig. 8, the concentration of HBV by PEI beads was improved by the addition of anti-HBV IgM antibody. Under the optimum condition, the number of viral copies obtained in the PEI bead fraction was more than seven-fold the number extracted from the untreated virus suspension even in the

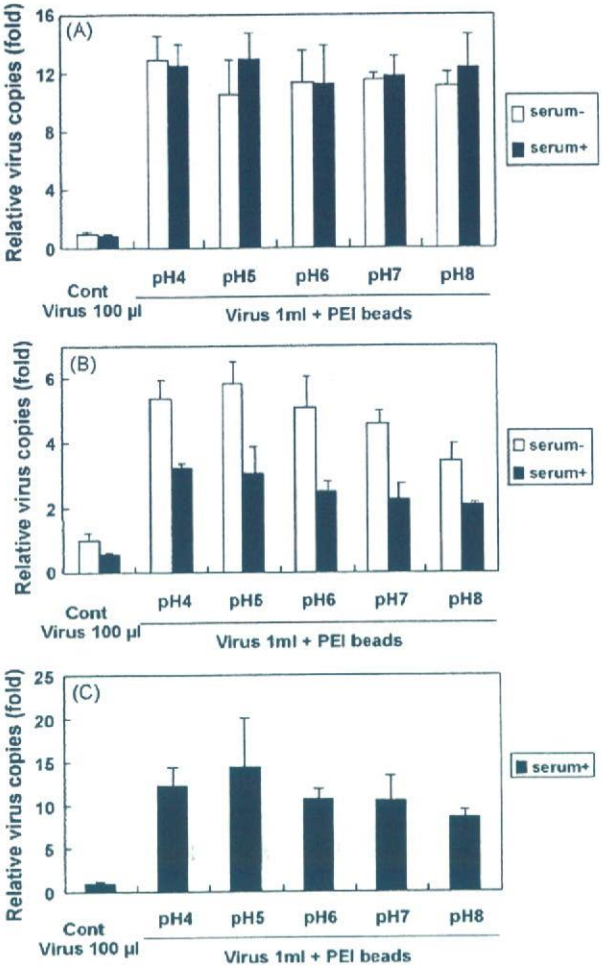

Fig. 7. Effect of pH on the concentration of HAV, HBV and HCV by PEI beads. HAV (A), HBV (B), and HCV (C) were diluted with virus dilution media of different pH levels supplemented with or without 2% FCS. Virus suspensions (HAV: 5×10^4 PFU/ml; HBV: 8.8×10^3 IU/ml; HCV: 1×10^3 IU/ml; 1 ml/tube) with different pH levels were incubated with PEI beads. Viral genome DNA and RNA were then extracted from PEI bead fraction and analyzed by real-time PCR and RT-PCR. Data are expressed as the mean ± S.D. ($n = 3$).

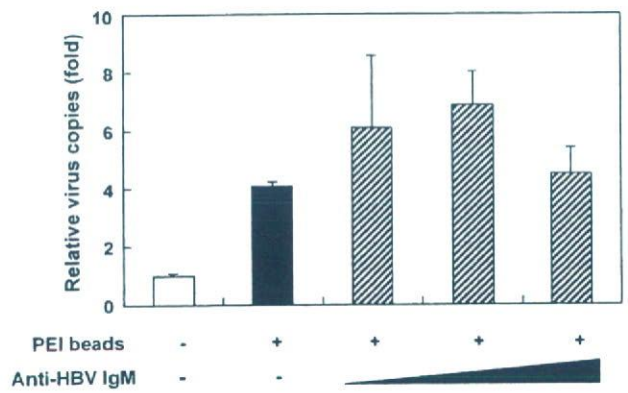

Fig. 8. Effect of anti-HBV IgM antibody for HBV concentration by PEI-beads. HBV suspensions (8.8×10^3 IU/ml; 1 ml/tube) were incubated with PEI beads in the absence or presence of 5, 15 or 50 µl of anti-HBV IgM antibody. Viral genome DNA was then extracted from the PEI bead fraction and analyzed by real-time PCR. Data are expressed as the mean ± S.D. ($n = 3$).

presence of serum. Therefore, the virus concentration achieved by PEI beads was shown to be enhanced by the formation of immune complexes.

Table 2 shows a summary of virus concentrations by PEI beads for all of the viruses examined. A wide range of viruses, including small non-enveloped viruses and human hepatitis viruses (HAV, HBV and HCV), were efficiently concentrated by PEI beads under the optimum condition, either directly or by the formation of immune complexes.

4. Discussion

In the present study, the virus concentration method using PEI beads (Satoh et al., 2003) was optimized, and was applied to human hepatitis A, B and C viruses.

First, the effects of various cationic polymers, PEI molecular weights, and pH values were examined in order to determine the optimal conditions for virus concentration. Among PEI beads with three different molecular weights (1800, 10,000 and 70,000 Da), only the PEI whose MW was 70,000 Da was able to adsorb viruses (Fig. 1). With respect to the cationic polymers, PEI magnetic beads showed a higher virus adsorption ability than PAA- or PLL-conjugated magnetic beads (Fig. 2). The optimum pH for the concentration of model viruses by PEI beads was subacidic (Fig. 3). The virus adsorption mechanism of PEI beads remains unclear. However, it is hypothesized that the positively charged field of the PEI molecule may interact tightly with the negative charge of surface lipids or the negatively charged surface proteins on viruses (Satoh et al., 2003). PEI is a polycationic polyamine with the highest cationic charge density among existing polymers (Futami et al., 2005). PEI has a branched backbone containing primary, secondary and tertiary amine groups. In contrast, PAA is a linear polycation having only primary amine groups, and PLL is a linear polycation with primary and secondary amine groups. Therefore, it is suggested that the high-density cationic charge of PEI and its branched structure on the surface of the magnetic beads may be important for efficient virus adsorption. According to the analysis of Owada et al. (1999), the interaction between PEI-coated membranes and human immunodeficiency virus type 1 (HIV-1) or plasma protein may be dependent on the surface area of each particle, and this fundamental principle was consistent with their observation that PEIs with higher MWs bound more intensely to HIV-1. This is also consistent with the data that PEI with a MW of 70,000 Da was able to adsorb viruses more efficiently than PEIs of 1800 Da or 10,000 Da.

In order to improve the efficiency of virus concentration by PEI beads, the serum components co-adsorbed by the beads were analyzed. MS analysis revealed that several proteins, including complement type 3, complement type 4 and IgM, were specifically co-adsorbed by PEI beads during virus concentration (Fig. 4), suggesting that the beads were able to adsorb immune complexes that involved IgM antibody and/or complements. Therefore, it is hypothesized that in addition to direct adsorption, PEI beads may adsorb viruses via the formation of immune complexes. This hypothesis was confirmed by the fact that PEI beads were able to adsorb poliovirus under con-

Table 2
Summary of concentration of viruses by PEI beads

Viruses	Natural host	Virus genome	Envelope	Size (nm)	PEI beads concentration
Model viruses cytomegalovirus (CMV)	Simian	DNA	+	180–200	+
Herpes symplex virus type 1 (HSV-1)	Human	DNA	+	150–200	+
Vesicular stomatitis virus (VSV)	Bovine	RNA	+	70–150	+
Amphotropic murine leukemia virus	Murine	RNA	+	80–110	+
Sindbis virus	Human	RNA	+	60–70	+
Adenovirus type 5	Human	DNA	–	70–90	+
Simian virus 40 (SV40)	Simian	DNA	–	40–50	+
Porcine parvovirus (PPV)	Porcine	DNA	–	18–24	+
Poliovirus sabin 1	Human	RNA	–	25–30	+[a]
Human hepatitis viruses hepatitis B virus (HBV)	Human	DNA	+	40–45	+[a]
Hepatitis C virus (HCV)	Human	RNA	+	40–50	+
Hepatitis A virus (HAV)	Human	RNA	–	25–30	+

[a] Concentrated by the addition of antibodies.

ditions which fostered immune complex formation, such as the addition of anti-poliovirus mouse IgG antibody with anti-mouse IgG rabbit IgM, or the addition of anti-poliovirus IgG antibody with activated complements (Fig. 6). Poliovirus is a very small (25–30 nm) non-enveloped virus, and could not be concentrated by PEI beads in our previous study (Satoh et al., 2003). Another possible explanation is that the increase in the surface area of virus particles due to the formation of immune complexes enhances the interaction between the poliovirus and the PEI beads, as hypothesized by Owada et al. (1999).

The results obtained from model viruses suggest that the virus concentration method using PEI beads may be applicable to a wide range of viruses. Therefore, this method was applied to human hepatitis viruses. A recent study reported that in some HAV patients, the duration of the viremic phase persisted for more than 1 year with low viral load levels (10^3–10^4 HAV genome equivalents/ml) (Normann et al., 2004). In the case of HBV, the presence of occult HBV infection (HBV DNA positivity in the setting of negative serum hepatitis B surface antigen) has been documented, and the majority of these infections were associated with low viral loads (<10^5 copies/ml) (Minuk et al., 2004). Several studies have demonstrated high rates of transmission of HCV through transfusions with extremely low viral loads (Operskalski et al., 2003). HCV is particularly infectious during the early window period, with levels as low as 1 viral copy in 20 ml plasma able to transmit infection by transfusion (Busch et al., 2003), though intermittent low-level HCV viremia can occur as long as 2 months before the periods of exponential increase in viral load (Glynn et al., 2005). Therefore, it is extremely important to develop a highly sensitive detection method for these viruses. In the present study, it was possible to concentrate HAV and HCV by PEI-beads to almost the predicted levels (Fig. 7). In contrast, HBV was not fully concentrated even under optimum conditions around pH 5. Therefore, the concentration of HBV via the formation of immune complexes was tested. As expected, the concentration of HBV was improved by the addition of anti-HBV IgM antibody (Fig. 8), indicating that the virus concentration method using PEI beads is applicable for the concentration and sensitive detection of HAV, HBV and HCV by PCR and RT-PCR reaction.

To enhance/establish the utility of this virus concentration method using PEI meads for viral safety of biological products and cell therapy products, examination using actual patient sera and different genotypes/subtypes of each virus may be required. In a preliminary experiment, it is confirmed that this PEI beads method can be used for hepatitis virus samples spiked in human plasma. Applicability to different genotypes will be examined using a Japanese genotype panel of HBV and HCV, which will be available soon.

PEI beads may be applicable not only for virus concentration but also for the efficient infection of viruses. Scherer et al. (2002) report that superparamagnetic nanoparticles coated with PEI enhanced the infection of adenovirus and retrovirus vectors under a magnetic field. This infection method (magnetofection) also enhanced the infection of measles virus (Kadota et al., 2005). In a preliminary experiment, the PEI beads used in the present study also enhanced the infectivity of several viruses under a magnetic field. Therefore, it is suggested that PEI beads may be useful for the sensitive detection of both virus genomes and virus infectivity.

In conclusion, the present study demonstrates that the virus concentration method using PEI beads is effective for the concentration and sensitive detection of a wide range of viruses, including HAV, HBV and HCV.

Acknowledgements

This work was supported in part by a Grant-in-Aid for Health and Labor Science Research (H17-SAISEI-021) from the Japanese Ministry of Health, Labor and Welfare, as well as by a Grant-in-Aid for Research on Health Sciences focusing on Drug Innovation from the Japan Health Sciences Foundation. The authors are grateful to Ms. Momoko Komesu for her technical assistance.

References

Alter, H.J., Sanchez-Pescador, R., Urdea, M.S., Wilber, J.C., Lagier, R.J., Di Bisceglie, A.M., Shih, J.W., Neuwald, P.D., 1995. Evaluation of branched DNA signal amplification for the detection of hepatitis C virus RNA. J. Viral Hepat. 2, 121–132.

Busch, M.P., Hirschkorn, D.F., Herring, B.L., Delwart, E.L., McAuley, J., Murthy, K.K., Alter, H.J., 2003. Defining the minimal infectious dose and infectious wind[o]w period for HCV using plasma donor panels and the chimpanzee transfusion model. Transfusion 43, S107–S140.

Futami, J., Kitazoe, M., Maeda, T., Nukui, E., Sakaguchi, M., Kosaka, J., Miyazaki, M., Kosaka, M., Tada, H., Seno, M., Sasaki, J., Huh, N.H., Namba, M., Yamada, H., 2005. Intracellular delivery of proteins into mammalian living cells by polyethylen[e]imine-cationization. J. Biosci. Bioeng. 99, 95–103.

Glynn, S.A., Wright, D.J., Kleinman, S.H., Hirschkorn, D., Tu, Y., Heldebrant, C., Smith, R., Giachetti, C., Gallarda, J., Busch, M.P., 2005. Dynamics of viremia in early hepatitis C virus infection. Transfusion 45, 994–1002.

Ishii-Watabe, A., Uchida, E., Iwata, A., Nagata, R., Satoh, K., Fan, K., Murata, M., Mizuguchi, H., Kawasaki, N., Kawanishi, T., Yamaguchi, T., Hayakawa, T., 2003. Detection of replication-competent adenoviruses spiked into recombinant adenovirus vector products by infectivity PCR. Mol. Ther. 8, 1009–1016.

Jothikumar, N., Cromeans, T.L., Sobsey, M.D., Robertson, B.H., 2005. Development and evaluation of a broadly reactive TaqMan assay for rapid detection of hepatitis A virus. Appl. Environ. Microbiol. 71, 3359–3363.

Kadota, S., Kanayama, T., Miyajima, N., Takeuchi, K., Nagata, K., 2005. Enhancing of measles virus infection by magnetofection. J. Virol. Meth. 128, 61–66.

Kamisango, K., Kamogawa, C., Sumi, M., Goto, S., Hirao, A., Gonzales, F., Yasuda, K., Iino, S., 1999. Quantitative detection of hepatitis B virus by transcription-mediated amplification and hybridization protection assay. J. Clin. Microbiol. 37, 310–314.

Kern, D., Collins, M., Fultz, T., Detmer, J., Hamren, S., Peterkin, J.J., Sheridan, P., Urdea, M., White, R., Yeghiazarian, T., Todd, J., 1996. An enhanced-sensitivity branched-DNA assay for quantification of human immunodeficiency virus type 1 RNA in plasma. J. Clin. Microbiol. 34, 3196–3202.

Martell, M., Gomez, J., Esteban, J.I., Sauleda, S., Quer, J., Cabot, B., Esteban, R., Guardia, J., 1999. High-throughput real-time reverse transcription-PCR quantitation of hepatitis C virus RNA. J. Clin. Microbiol. 37, 327–332.

Minuk, G.Y., Sun, D.F., Greenberg, R., Zhang, M., Hawkins, K., Uhanova, J., Gutkin, A., Bernstein, K., Giulivi, A., Osiowy, C., 2004. Occult hepatitis B virus infection in a North American adult hemodialysis patient population. Hepatology 40, 1072–1077.

Mizusawa, S., Okada, Y., Horiuchi, Y., Tanaka, T., Sato, K., Kaneko, K., Sasaki, Y., Tanaka, T., Tomono, T., Tomomizu, T., Hayami, S., Hijikata, M., Hirako, I., Mayumi, M., Mikami, K., Mishiro, S., Miyamoto, S., Muta, K., Weimer, T., Gierman, T., Komuro, K., Yamaguchi, T., 2005. Establishment of the first national standard for nucleic acid amplification technology assay for HCV RNA. Jpn. J. Transfus. Med. 51, 515–519.

Normann, A., Jung, C., Vallbracht, A., Flehmig, B., 2004. Time course of hepatitis A viremia and viral load in the blood of human hepatitis A patients. J. Med. Virol. 72, 10–16.

Notomi, T., Okayama, H., Masubuchi, H., Yonekawa, T., Watanabe, K., Amino, N., Hase, T., 2000. Loop-mediated isothermal amplification of DNA. Nucl. Acids Res. 28, E63.

Operskalski, E.A., Mosley, J.W., Tobler, L.H., Fiebig, E.W., Nowicki, M.J., Mimms, L.T., Gallarda, J., Phelps, B.H., Busch, M.P., 2003. HCV viral load in anti-HCV-reactive donors and infectivity for their recipients. Transfusion 43, 1433–1441.

Owada, T., Miyashita, Y., Motomura, T., Onishi, M., Yamashita, S., Yamamoto, N., 1999. Anti-HIV-1 activity of an ionically modified porous polypropylene membrane determined by filtration of a viral suspension. Microbiol. Immunol. 43, 141–151.

Pas, S.D., Fries, E., De Man, R.A., Osterhaus, A.D., Niesters, H.G., 2000. Development of a quantitative real-time detection assay for hepatitis B virus DNA and comparison with two commercial assays. J. Clin. Microbiol. 38, 2897–2901.

Saiki, R.K., Gelfand, D.H., Stoffel, S., Scharf, S.J., Higuchi, R., Horn, G.T., Mullis, K.B., Erlich, H.A., 1988. Primer-directed enzymatic amplification of DNA with a thermostable DNA polymerase. Science 239, 487–491.

Sarrazin, C., Teuber, G., Kokka, R., Rabenau, H., Zeuzem, S., 2000. Detection of residual hepatitis C virus RNA by transcription-mediated amplification in patients with complete virologic response according to polymerase chain reaction-based assays. Hepatology 32, 818–823.

Satoh, K., Iwata, A., Murata, M., Hikata, M., Hayakawa, T., Yamaguchi, T., 2003. Virus concentration using polyethyleneimine-conjugated magnetic beads for improving the sensitivity of nucleic acid amplification tests. J. Virol. Meth. 114, 11–19.

Scherer, F., Anton, M., Schillinger, U., Henke, J., Bergemann, C., Kruger, A., Gansbacher, B., Plank, C., 2002. Magnetofection: enhancing and targeting gene delivery by magnetic force in vitro and in vivo. Gene Ther. 9, 102–109.

Uchida, E., Sato, K., Iwata, A., Ishii-Watabe, A., Mizuguchi, H., Hikata, M., Murata, M., Yamaguchi, T., Hayakawa, T., 2004. An improved method for detection of replication-competent retrovirus in retrovirus vector products. Biologicals 32, 139–146.

Willkommen, H., Schmidt, I., Lower, J., 1999. Safety issues for plasma derivatives and benefit from NAT testing. Biologicals 27, 325–331.

Leukemia (2007), 1–10

www.nature.com/leu

ORIGINAL ARTICLE

Proteome analyses of the growth inhibitory effects of NCH-51, a novel histone deacetylase inhibitor, on lymphoid malignant cells

T Sanda[1,2], T Okamoto[1], Y Uchida[1], H Nakagawa[3], S Iida[2], S Kayukawa[2], T Suzuki[3], T Oshizawa[4], T Suzuki[4], N Miyata[3] and R Ueda[2]

[1]Department of Molecular and Cellular Biology, Nagoya City University Graduate School of Medical Sciences, Nagoya, Japan; [2]Department of Internal Medicine and Molecular Science, Nagoya City University Graduate School of Medical Sciences, Nagoya, Japan; [3]Department of Organic and Medicinal Chemistry, Nagoya City University Graduate School of Pharmaceutical Sciences, Nagoya, Japan and [4]Department of Cellular and Gene Therapy Products, National Institute of Health Sciences, Tokyo, Japan

Recent reports showing successful inhibition of cancer and leukemia cell growth using histone deacetylase inhibitor (HDACi) compounds have highlighted the potential use of HDACi as anti-cancer agents. However, high incidence of toxicity and low stability *in vivo* were observed with hydroxamic acid-based HDACi such as suberoylanilide hydroxamic acid (SAHA), thus limiting its clinical applicability. In this study, we found that a novel non-hydroxamate HDACi NCH-51 could inhibit the cell growth of a variety of lymphoid malignant cells through apoptosis induction, more effectively than SAHA. Activation of caspase-3, -8 and -9, but not -7 was detected after the treatment with NCH-51. Gene expression profiles showed that NCH-51 and SAHA similarly upregulated *p21* and downregulated anti-apoptotic molecules including *survivin*, *bcl-w* and *c-FLIP*. Proteome analysis using two-dimensional electrophoresis revealed that NCH-51 upregulated anti-oxidant molecules including peroxiredoxin 1 and 2 and glutathione *S*-transferase at the protein level. Interestingly, NCH-51 induced reactive oxygen species (ROS) after 8 h whereas SAHA continuously declined ROS. Pretreatment with an antioxidant, *N*-acetyl-L-cysteine, abolished the cytotoxicity of NCH-51. These findings suggest that NCH-51 exhibits cytotoxicity by sustaining ROS at the higher level greater than SAHA. This study indicates the therapeutic efficacy of NCH-51 and novel insights for anti-HDAC therapy.

Leukemia advance online publication, 9 August 2007; doi:10.1038/sj.leu.2404902

Keywords: histone deacetylase; apoptosis; reactive oxygen species; peroxiredoxin

Introduction

Histone deacetylase (HDAC) is responsible for deacetylation of histone or non-histone substrates.[1–3] Deacetylation of histone converts local chromatin into repressive configuration, resulting in the transcriptional repression.[2,3] The aberrant recruitment of HDAC is closely associated with leukemogenesis through silencing of expression of the genes involved in hematopoietic cell differentiation.[4] In addition, subsequent studies demonstrated that the malignant phenotypes of solid tumors could be ascribed to the aberrant activation of HDAC and deacetylation of the histone proteins adjacent to tumor suppressor genes.[5,6] Thus, a number of small-molecule HDAC inhibitors (HDACi) have been developed as anti-cancer agents.[1,7] In fact, HDACi compounds were shown to induce cell cycle arrest, differentiation and apoptosis in a variety of malignant cells.[1,7]

Suberoylanilide hydroxamic acid (SAHA) (also known as vorinostat) belongs to a hydroxamic acid-based hybrid polar compound and is a prototypic compound of HDACi.[7] Phase I clinical trials with refractory solid tumors and hematological malignancies by SAHA revealed frequent toxicities including dehydration, fatigue, diarrhea, anorexia and cytopenia, in spite of significant clinical benefits.[8] In addition, a poor pharmacokinetics of SAHA was noted.[8] Other hydroxamic acid-based derivatives showed similar therapeutic profiles.[9,10] Thus, we have attempted to develop a non-hydroxamate HDACi to overcome these problems. A novel HDACi NCH-51 was designed based on SAHA by replacement of the hydroxamic acid by acylated thiol group. NCH-51 could inhibit HDACs as strongly as SAHA and inhibited the cell growth of various solid tumor cell lines *in vitro* (mean IC_{50} values of NCH-51 and SAHA are 3.8 and 3.7 μM, respectively).[11] Unlike SAHA, NCH-51 is stable in human plasma at the remaining rate of approximately 51% after 24 h of administration (unpublished data).

Recent findings suggest that HDACi may have additional effects other than transcriptional interference. Although it is well established that HDACi upregulates gene expression of tumor suppressors such as *p21* through histone hyperacetylation,[12–14] HDACi does not always upregulate gene expression but induces malignant cell death by downregulating gene expression such as anti-apoptotic genes. In addition, some HDACi compounds exhibited anti-cancer effects through acetylation of non-histone substrates such as heat-shock protein 90 (HSP90),[15] α-tubulin,[16] p53[17] and nuclear factor-κB.[18] For example, Bali *et al.*[15] reported that HDACi caused leukemia cell death by hyperacetylation of HSP90. Hideshima *et al.*[19] demonstrated that tubacin, a specific HDAC6 inhibitor, was effective in augmenting cell death mediated by bortezomib, a proteasome inhibitor, by inhibiting the protein degradation through blocking aggresome activity. Thus, the cell growth inhibitory action of HDACi could be exhibited at the protein expression level.

Here we demonstrate the therapeutic efficacy of NCH-51 on lymphoid malignant cells. NCH-51 induced cell death, more strongly than SAHA. We analyzed the protein expression profiles and found that NCH-51 modulated the expression of antioxidant molecules at the protein level. NCH-51 sustained the intracellular reactive oxygen species (ROS) greater than SAHA.

Correspondence: Professor T Okamoto, Department of Molecular and Cellular Biology, Nagoya City University Graduate School of Medical Sciences, 1 Kawasumi, Mizuho-cho, Mizuho-ku, Nagoya, Aichi 467-8601, Japan.
E-mail: tokamoto@med.nagoya-cu.ac.jp
Received 22 March 2007; revised 6 June 2007; accepted 11 July 2007

a

Cell type		Cell line name	24h		72h	
			SAHA	NCH-51	SAHA	NCH-51
T-cell	T-ALL	Jurkat	0.90	0.72	0.63	0.75
	ATL	MT-2	>30.00	7.81	0.54	2.08
		ATL-102	>30.00	5.80	3.70	2.25
		ED-40515 (-)	1.45	0.94	0.90	0.76
B-cell	CLL	MEC2	>30.00	0.71	0.70	0.67
		MO1043	>30.00	7.67	0.76	0.79
	BL	Raji	>30.00	1.65	0.84	0.71
		Daudi	>30.00	>30.00	>30.00	11.74
	MM	U266	7.67	1.36	0.53	0.66
		XG7	>30.00	2.00	0.73	1.11
		KMS	>30.00	>30.00	1.35	3.49
		ILKM-2	1.41	1.11	0.61	0.66
		RPMI8226	5.72	2.92	2.92	2.72

Growth inhibition (%)
80-100
60-80
40-60
20-40
0-20
Each Value means IC_{50}

b

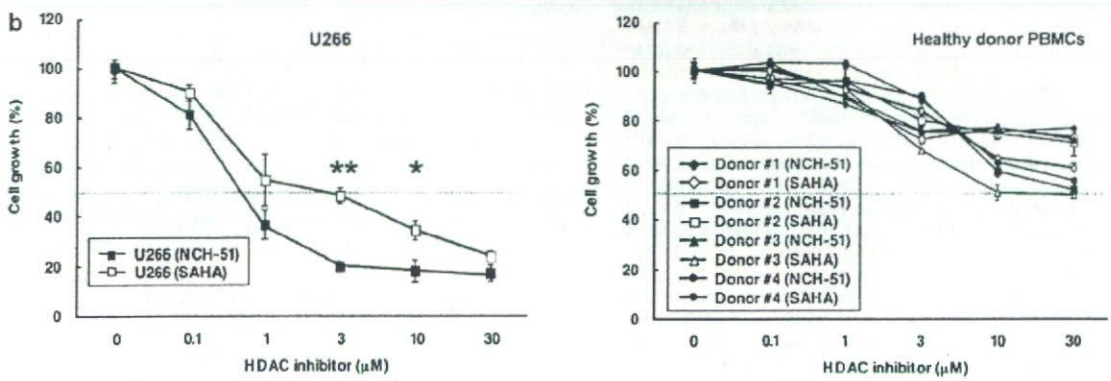

c

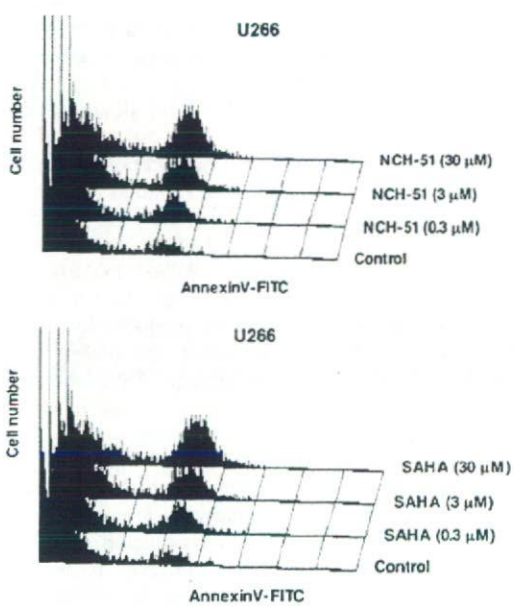

d

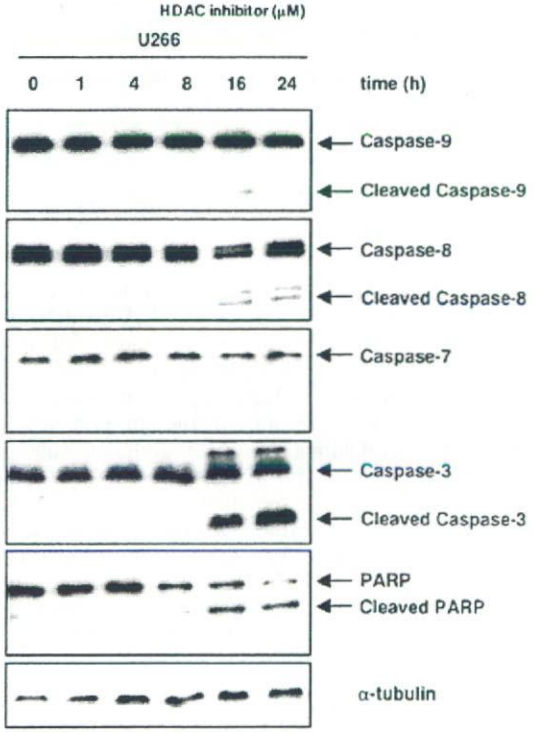

Materials and methods

Cell lines and reagents

A human acute T-cell leukemia cell line, Jurkat, ATL cell lines, MT-2, ATL-102 and ED-40515(−), chronic lymphocytic leukemia cell lines, MEC2 and MO1043, Burkitt's lymphoma cell lines, Raji and Daudi and multiple myeloma cell lines, U266, XG7, KM5, ILKM-2 and RPMI-8226 were used in this study as described previously.[20–24] For normal controls, peripheral blood mononuclear cells (PBMCs) were obtained from four independent healthy donors upon informed consent after the approval of Institutional Ethical Committee. All cells were cultured in RPMI-1640 medium, supplemented with 10% fetal bovine serum at 37°C in a 5% CO_2 incubator. NCH-51, a novel non-hydroxamate HDACi, and SAHA, a conventional hydroxamate HDACi, were synthesized by us as described previously.[11] NCH-51 and SAHA were dissolved in dimethyl sulfoxide at 50 mM and stored at −20°C. An antioxidant compound *N*-acetyl-L-cysteine (NAC) was purchased from Sigma (St Louis, MS, USA).

Growth inhibition assay

Growth inhibitory effect of HDACi was determined using 3-(4,5-dimethylthiazol-2-yl)-2,5-diphenyltetrazolium bromide assay (Sigma) as described previously.[25] Briefly, approximately $1–10 \times 10^4$ cells per 100 μl were cultured in 96-well plate in triplicates at 37°C. Optical densities (OD) at 570 and 630 nm were measured with a multiplate reader. Cell growth (%) was calculated as follows: (OD_{630}–OD_{570} of the samples/OD_{630}–OD_{570} of the control) × 100.

Apoptosis and cell cycle analysis

Apoptosis and cell cycle analyses were performed as described previously.[20] For apoptosis analysis, the cells were treated with or without HDACi for 18 h, and incubated with fluorescein isothiocyanate (FITC)-conjugated annexin V (MBL, Nagoya, Japan). The cell numbers of annexin V-positive cells were analyzed by flowcytometry (FACScan, BD Bioscience, San Jose, CA, USA) and CellQuest analysis program (BD Bioscience). For cell cycle analysis, the cells were incubated with or without HDACi for 24 h, washed with cold phosphate-buffered saline (PBS), and fixed with 70% ethanol. After incubation with RNase A (Qiagen, Alameda, CA, USA), the cell pellets were resuspended in PBS containing propidium iodide (Sigma). DNA content of each cell preparation was analyzed by flowcytometry.

Protein extraction for proteome analysis

Proteome analysis was performed according to Seike *et al.*[26] U266 cells were incubated with or without 3 μM NCH-51 for 18 h. The cell pellets were washed with cold PBS and then treated with 10%trichloroacetic acid for 30 min on ice. After washing with PBS, the pellets were collected and resuspended in lysis buffer (30 mM Tris–HCl (pH, 8.5), 7 M urea, 2 M thiourea, 3% 3-((3-chlamidopropyl) dimethylammonio)-1-propanesulfonic acid and 1% Triton X-100). Samples were then subjected to a Dounce homogenizer for 30 strokes and sonicated for 5 min in a sonicator (UCW-201, Cosmobio Co. Ltd., Tokyo, Japan). After incubation for 30 min, the samples were centrifuged at $10\,000 \times g$ for 30 min followed by ultracentrifugation at $100\,000 \times g$ for 1 h, and the supernatants were collected. Protein concentration was determined by 2D-Quant kit (GE Healthcare Bio-Sciences Corp., Piscataway, NJ, USA). Fifty micrograms of each protein extract, adjusted to pH 8.5, were labeled with 200 pmol of minimal dye CyDye (GE Healthcare Bio-Sciences Corp.). NCH-51-treated samples and untreated control proteins were labeled with Cy3 and Cy5, respectively. Internal control, consisting of half part of each paired sample was labeled with Cy2. Labeling reaction was stopped with the addition of 0.2 mM L-lysine (Sigma) for 10 min on ice. Each labeled sample was mixed into one tube and then incubated with an equal amount of lysis buffer for 10 min on ice. The final volume was adjusted to 450 μl with DeStreak Rehydration Solution and 0.5% IPG buffer (GE Healthcare Bio-Sciences Corp.).

Two-dimensional (2D) electrophoresis and image analysis

An immobilized pH gradient gel Immobiline DryStrip (GE Healthcare Bio-Sciences Corp.), with non-linear pH values (3–10), was rehydrated with the labeled protein samples at 20°C for 12 h. Isoelectric focusing was performed using IPGphor (GE Healthcare Bio-Sciences Corp.) at 20°C for total 65 000 khT. Immobiline DryStrips were then equilibrated for 15 min in the buffer (6 M urea, 1.5 M Tris–HCl (pH 8.8), 30% glycerol, 2% sodium dodecyl sulfate) containing 10 mg/ml dithiothreitol and prolonged for 15 min in the same buffer containing 25 mg/ml iodoacetamide. After equilibration, Immobiline DryStrips were transferred onto 11.5% polyacrylamide gels and run in the EttanDalt Six system (GE Healthcare Bio-Sciences Corp.) at 30 W/gel for 5 h at 20°C. The gels were scanned with appropriate wavelengths for excitation and emission using Ettan DIGE Primo (GE Healthcare Bio-Sciences Corp.). Relative quantification of spot intensities and statistical evaluation were carried out with ImageMaster 2D Platinum software (GE Healthcare Bio-Sciences Corp.). The experiments were performed in quadruplicates. The protein spots that were statisti-

Figure 1 Induction of apoptosis by a novel HDAC inhibitor NCH-51. (**a**) The growth inhibitory effects of NCH-51 and suberoylanilide hydroxamic acid (SAHA) on 13 lymphoid malignant cell lines. The cells were treated with either NCH-51 or SAHA (3 μM) for 24 or 72 h. Cell growth was estimated by 3-(4,5-dimethylthiazol-2-yl)-2,5-diphenyltetrazolium bromide (MTT) assay and gray-scale levels represent the growth inhibition rate (%) compared to untreated control. Each value indicates the mean IC_{50}. (**b**) Growth inhibitory effects of NCH-51 and SAHA on U266 cells and four control peripheral blood mononuclear cells (PBMCs). A multiple myeloma cell line U266 cells, and four healthy donor PBMCs were treated with indicated concentrations (0–30 μM) of NCH-51 (closed symbols) or SAHA (opened symbols) for 24 h. Cell growth was evaluated by MTT assay. The results are shown as the percentage cell growth compared to untreated control. These experiments were performed in triplicates and the mean values ± s.d. are shown. *$P<0.05$; **$P<0.01$. (**c**) Induction of apoptosis by NCH-51. U266 cells were treated with the indicated concentrations (0–30 μM) of NCH-51 for 18 h, stained with fluorescein isothiocyanate-conjugated annexin V, and analyzed by flowcytometry. Annexin V-positive fraction indicates the cells undergoing apoptosis. (**d**) Activation of caspases and poly-ADP ribose polymerase (PARP) cleavage by NCH-51. U266 cells were treated with 3 μM of NCH-51 for 0–24 h. Whole cell extracts were prepared and subjected to immunoblots with the indicated antibodies. Positions of uncleaved (inactivated) and cleaved (activated) caspases and PARP proteins are indicated by arrows.

cally significant between untreated control and treated sample were selected.

Protein identification by mass spectrometry

For mass spectrometric analysis, 400 μg of unlabeled-protein extract was independently applied to 2D electrophoresis. The gel was stained with DeepPurple solution (GE Healthcare Bio-Sciences Corp.) according to the manufacturer's recommendation. The gel image was obtained by scanning with Ettan DIGE Primo and matched to those of analytical gels by using the ImageMaster 2D Platinum software. The spots of interest were picked out, and in-gel protein digestion was carried out with trypsin gold (Promega, Madison, WI, USA) as described.[26] Mass spectrometric analyses were performed by using a MALDI-TOF/TOF type mass spectrometer AB4700 (Applied Biosystems, Framingham, MA, USA). The proteins were identified through the online search using MASCOT database search engine.

Immunoblot analysis

The cell extracts obtained from cell cultures treated with or without HDACi were subjected to cell extract preparation as described above. The samples were applied to electrophoresis on a 10% polyacrylamide gel and transferred onto a nitrocellulose membrane. The membranes were incubated in TBS-T (10 mM Tris–HCl (pH, 8.0), 150 mM NaCl, 0.1% Tween) with 5% non-fat milk containing 1:1000 diluted primary antibodies against either caspase-9, -8, -7, -3, poly-ADP ribose polymerase (PARP) (Cell Signaling Technology, Danvers, MA, USA), peroxiredoxin 1 (Affinity Bioreagents, Golden, CO, USA), elongation factor-2 or α-tubulin (Santa Cruz, Santa Cruz, CA, USA). Membranes were then rinsed in TBS-T and further incubated with HRP-conjugated secondary antibody (GE Healthcare Bio-Sciences Corp.) in TBS-T with 5% non-fat milk. Each protein was detected by SuperSignal (PIERCE, Rockford, IL, USA).

Detection of ROS

ROS content was measured as described previously.[27] After treatment with HDACi, the cells were incubated with an oxidation-sensitive fluorescent probe 2′, 7′-dichlorofluorescein diacetate (H_2-DCFDA) (Molecular Probes Inc., Eugene, OR, USA) at a final concentration of 5 μM for 30 min. The cells were washed and resuspended in PBS, and then ROS amount was measured by flowcytometry.

Results

NCH-51 induces apoptosis greater than SAHA

We first evaluated the growth inhibitory effects of NCH-51 on a variety of lymphoid malignant cell lines (Figure 1a). A tentative result in a multiple myeloma cell line U266 cells is shown in Figure 1b. In most of the cell lines including U266 cells, NCH-51 exhibited a stronger growth inhibitory effect than SAHA at 3 μM for 24 h treatment, whereas prolonged incubation for 72 h did not show such a difference. It is noted that there was no significance in the growth inhibitory effect on four healthy donor PBMCs between NCH-51 and SAHA (IC_{50} values of both agents were higher than 30 μM), suggesting a cell-type specific cytotoxicity of NCH-51. We then analyzed the apoptosis and cell cycle distribution after the treatment with NCH-51 or SAHA. In the six cell lines (Jurkat, ED-40515(−), MEC2, U266, XG7 and ILKM-2), all of which showed a high susceptibility to NCH-51 ($IC_{50}<3$ μM), NCH-51 strongly induced apoptosis greater than SAHA after 24 h treatment as demonstrated by generation of sub-G_1 cells (Figure 1c and Table 1). In fact, when U266 cells were treated with NCH-51, cleaved forms of caspase-9, -8, -3 and PARP could be detected after 8 h, evidently at 16 h, although no activation of caspase-7 was detected (Figure 1d), suggesting that NCH-51 induces apoptosis through both extrinsic (type I) and intrinsic (type II) pathways[28] in the short-term treatment. On the other hand, cell cycle analysis revealed that NCH-51 increased the cell number at G_2/M-phase and reduced the number at G_1- or S-phase in most of the cell lines examined (Table 1, right column). No significant difference in the effects on cell cycle regulation was observed between NCH-51- and SAHA-treated cells. These observations suggest that the apoptosis-inducing activity might be attributable to the difference in the observed growth inhibitory effects between NCH-51 and SAHA.

NCH-51 regulates the expressions of antioxidant molecules at the protein level

To identify the target molecules regulated by NCH-51, we analyzed the RNA and protein expression profiles. cDNA microarray analysis using U266 cells showed that NCH-51 treatment upregulated the expression of *p21* and *p19* (Supplementary Table 1), confirming the previous reports by us[11] and others.[12–14] On the other hand, NCH-51 downregulated the gene expression of *CFLAR* (*c-FLIP*), *survivin* and *BCL2L2 (bcl-w)*, which act as antiapoptotic molecules. These results suggested that these genes were responsible for the growth inhibitory action of NCH-51, however, there was no notable difference in mRNA expression between NCH-51- and SAHA-treated cells. We then performed the proteome analysis. Whole cell extracts were prepared from U266 cells treated with or without NCH-51, and the protein samples were labeled with fluorescent dyes and applied to 2D electrophoresis (Figure 2a). By comparing the amounts of cellular proteins, we identified 14 proteins that varied relatively to NCH-51 treatment (Table 2). Ten proteins including nucleotide diphosphate kinase A (NDPKA), peroxiredoxin 1 and 2 (PRDX1, 2), glutathione *S*-transferase P1-1 (GSTP1-1), 14-3-3 zeta/delta, Cl^- intracellular channel proteins 1 and 4 (CLIC1, 4), proteasome subunit α3, protease activator 28 β subunit and Rho GDI α were upregulated, and four proteins including alanyl-tRNA synthetase (AARS), elongation factor-2 (EF-2), heat-shock 70 kDa protein 8 (HSPA8) and mitochondrial inner membrane protein, were downregulated after the treatment with NCH-51. Interestingly, some of these proteins upregulated by NCH-51 belong to a class of antioxidant molecules. It is noted that PRDX1 and PRDX2 were upregulated at both mRNA and protein levels, thus they are considered to be upregulated at the gene expression level, whereas most of the proteins were upregulated without induction at the gene expression level. In contrast, EF-2 and HSPA8 were downregulated at the protein level. The effects of NCH-51 and SAHA on the expression of EF-2 and PRDX1 were then verified. As shown in Figure 2b, EF-2 protein level was decreased either by NCH-51 or SAHA in the cell lines such as U266, ED-40515 (−) and XG7 cells that were highly susceptible to HDACi. EF-2 was decreased after 16 h treatment with these HDACi (data not shown). On the other hand, in the cell lines such as MEC2, Daudi and KM5 cells that were less sensitive to HDACi, EF-2 protein level was not significantly changed. PRDX1 protein level was upregulated by the treatment with either NCH-51 or SAHA in ED-40515 (−), U266, XG7 and MEC2 cells. SAHA seemed to upregulate PRDX1 more than NCH-51.

Table 1 The profiles of apoptosis and cell cycle distribution

Cell line	*HDAC inhibitor (μM)*	*Apoptotic cell[a] (%)*	*Cell cycle distribution[a](%)*			
			sub G_1	*G_1*	*S*	*G_2/M*
Jurkat	Untreated control	6.30	5.11	50.39	20.76	20.64
	SAHA					
	3 μM	13.45	28.56	9.15	12.97	46.22
	30 μM	28.97	32.39	7.06	18.10	40.83
	NCH-51					
	3 μM	19.27	42.66	8.05	10.04	36.28
	30 μM	35.45	42.69	7.64	14.41	32.21
MT-2	Untreated control	6.84	3.02	63.25	15.29	15.64
	SAHA					
	3 μM	8.23	9.41	49.04	11.70	26.36
	30 μM	8.75	10.35	62.95	6.15	13.96
	NCH-51					
	3 μM	8.45	3.26	62.21	16.34	16.53
	30 μM	8.62	5.38	71.64	8.35	12.22
ED-40515 (−)	Untreated control	6.44	8.40	46.82	23.30	19.67
	SAHA					
	3 μM	20.74	18.88	21.41	19.07	36.90
	30 μM	20.12	26.87	22.20	20.49	27.75
	NCH-51					
	3 μM	22.12	27.10	28.04	19.04	23.91
	30 μM	21.33	26.54	25.09	20.56	25.72
MEC2	Untreated control	3.20	5.66	60.06	19.96	12.16
	SAHA					
	3 μM	4.84	12.32	37.33	19.84	26.70
	30 μM	8.22	18.14	29.46	22.63	25.12
	NCH-51					
	3 μM	6.50	16.22	36.43	19.28	24.75
	30 μM	11.08	21.24	30.47	20.93	23.29
MO1043	Untreated control	4.14	0.89	54.88	20.75	17.87
	SAHA					
	3 μM	4.30	3.45	68.83	7.49	15.41
	30 μM	15.96	18.85	48.29	6.62	23.14
	NCH-51					
	3 μM	3.74	2.47	73.90	7.17	12.88
	30 μM	14.93	21.75	48.79	6.14	21.03
Daudi	Untreated control	1.62	1.62	52.02	22.77	19.55
	SAHA					
	3 μM	2.08	2.17	23.65	22.33	46.30
	30 μM	2.12	2.34	22.83	19.75	48.21
	NCH-51					
	3 μM	2.64	1.90	50.38	14.74	27.71
	30 μM	3.04	2.19	25.68	22.19	43.28
U266	Untreated control	6.17	6.30	67.42	10.99	13.02
	SAHA					
	3 μM	17.65	11.91	56.24	10.35	19.72
	30 μM	29.73	17.06	48.70	12.69	19.68
	NCH-51					
	3 μM	22.90	13.39	54.07	11.60	18.62
	30 μM	32.63	18.90	49.15	13.40	18.94
XG7	Untreated control	7.27	7.58	49.21	20.34	23.37
	SAHA					
	3 μM	8.74	8.50	50.40	8.33	28.32
	30 μM	9.43	15.38	34.23	15.10	28.21
	NCH-51					
	3 μM	11.47	10.00	49.32	8.62	28.62
	30 μM	13.13	17.87	35.44	14.67	27.93
KM5	Untreated control	4.24	2.91	42.15	27.85	23.43
	SAHA					
	3 μM	4.30	6.32	31.85	31.44	26.13
	30 μM	15.96	23.37	20.62	26.19	24.68
	NCH-51					
	3 μM	3.74	6.75	38.34	29.96	20.84
	30 μM	18.46	20.33	27.77	23.29	24.31

Table 1 (*Continued*)

Cell line	HDAC inhibitor (μM)	Apoptotic cell[a] (%)	Cell cycle distribution[a](%)			
			sub G_1	G_1	S	G_2/M
ILKM-2	Untreated control	7.35	4.07	58.61	13.05	22.89
	SAHA					
	3 μM	7.84	8.97	61.53	6.23	22.12
	30 μM	21.41	20.63	51.10	12.71	13.88
	NCH-51					
	3 μM	8.71	6.04	63.21	6.93	22.45
	30 μM	30.04	20.54	51.45	12.15	15.13

Abbreviations: HDAC, histone deacetylase; SAHA, suberoylanilide hydroxamic acid.
[a]Each value shows the average of 20 000 cells counted.

NCH-51 induces cytotoxic effect through the modulation of intracellular ROS

From the results of proteome analyses, NCH-51 appeared to promote the expression of antioxidant molecules, either at the transcriptional or post-transcriptional level, which prompted us to examine the effect of NCH-51 on the levels of ROS accumulation. Interestingly, the temporal profile of ROS amount in U266 cells treated with NCH-51 appeared to be in a concave shape indicating a gradual suppression of ROS accumulation within the initial 4 h and subsequent induction of ROS (Figure 3a), whereas the temporal profile with SAHA continuously declined over time. Similar trends were observed with other cell lines (data not shown). As summarized in Table 2, SAHA was more effective in reducing ROS than NCH-51, and the difference in ROS amount between NCH-51 and SAHA was most evident at 24 h, when the difference in growth inhibitory effect could be observed (Figure 1). These results suggested a possibility that dynamic state of ROS in each cell could be attributed to the growth inhibitory effect of HDACi. We thus examined whether NAC, a small-molecule antioxidant compound, could modulate the effect of NCH-51 (Figure 3b). Expectedly, when U266 cells were pretreated with NAC, the NCH-51-mediated cell growth inhibition was abolished. Similar effect was observed in SAHA-treated cells as much as in NCH-51-treated cells (data not shown). These results indicated that high amount of ROS might be necessary for the induction of NCH-51-mediated cytotoxicity.

Discussion

There have been accumulating reports of successful inhibition of cancer cell growth using small-molecule HDACi compounds.[1,7] Initial studies with SAHA indicated that the mode of action of HDACi might be through upregulating the transcriptionally repressed genes during carcinogenic processes by acetylating the repressive histones.[12–14] However, recent reports have demonstrated that HDACi compounds also exert anticancer effects through acetylation of non-histone substrates.[15–19] For example, HDAC6, a microtubule-associated deacetylase, was shown to be responsible for transportation of misfolded proteins to aggresome thus promoting protein degradation.[19,29] Thus, we have attempted to clarify the mechanism of anticancer effects of NCH-51 by examining both mRNA and protein levels.

In this study, we noticed that NCH-51 induced apoptosis in sensitive cell lines greater than SAHA (Figures 1 and 2a and Table 1). Analyses of mRNA expression levels in NCH-51- and SAHA-treated cells has revealed that transcriptional repression of antiapoptotic genes, such as *survivin*, *bcl-w* and *c-FLIP* and upregulation of cell cycle regulators, such as *p21* and *p19*, could be attributable to the induction of apoptosis and cell cycle arrest, respectively (Supplementary Table 1, 2 and Supplementary Figure 1), supporting the previous findings by others.[12–14] There was no difference in the mRNA expression level between NCH-51- and SAHA-treated samples (Supplementary Figure 1). We have confirmed no difference in inducing activity for acetylation of histone H4 between these two HDACi's (Supplementary Figure 2). These findings suggest that NCH-51 and SAHA similarly affect gene expression presumably through histone acetylation. We thus examined the effects of these compounds on protein expression profile to understand the difference between NCH-51 and SAHA at the post-transcriptional level.

Interestingly, our proteome analyses revealed the upregulation of some antioxidant molecules including PRDX1, PRDX2 and GSTP1-1 (Table 2 and Figure 2). In addition, previous reports indicated that some other proteins identified by the present proteome analysis (Table 2) could be activated by oxidative stress.[30–34] For example, NDPKA is reported to be activated by ROS and protected the cell from ROS-induced apoptosis.[30,31] CLIC1 protein contains a redox-active site and is activated during ROS-triggered apoptosis.[32,33] These findings suggested a possibility that NCH-51 might induce the cytotoxic effect by modulating the intracellular ROS content. In fact, pretreatment with NAC abolished the growth inhibitory effect of NCH-51 (Figure 3b). These results support the previous findings by others, which showed the ROS accumulation by HDACi.[14,34,35] However, in contrast to the previous reports, both NCH-51 and SAHA downregulated the ROS content after 24 h treatment in most of the cell lines tested except for KM5 cells, in which ROS was increased by the treatment with SAHA or NCH-51 (Table 3). These findings were reproducibly observed. Although we currently do not know the reason why there was a discrepancy between our study and others, we think the time-point and/or cell characteristics may be different between them. When temporal profiles of ROS accumulation were examined (Figure 3a), we found a typical bimodal kinetics of the intracellular ROS content after treatment with NCH-51; an initial downregulation and subsequent upregulation of ROS. On the other hand, SAHA did not follow the similar kinetics and the intracellular ROS level gradually and continuously decreased (Figure 3a). Therefore, it is possible that apparent differences in the ability of cell growth inhibition between NCH-51 and SAHA, may be explained through the different effects on the redox status of cells and induction of antioxidant proteins. Interestingly, our proteome/transcriptome analyses have revealed that the upregulation of antioxidant molecules occurred at either protein or mRNA levels: GSTP1-1 was upregulated by

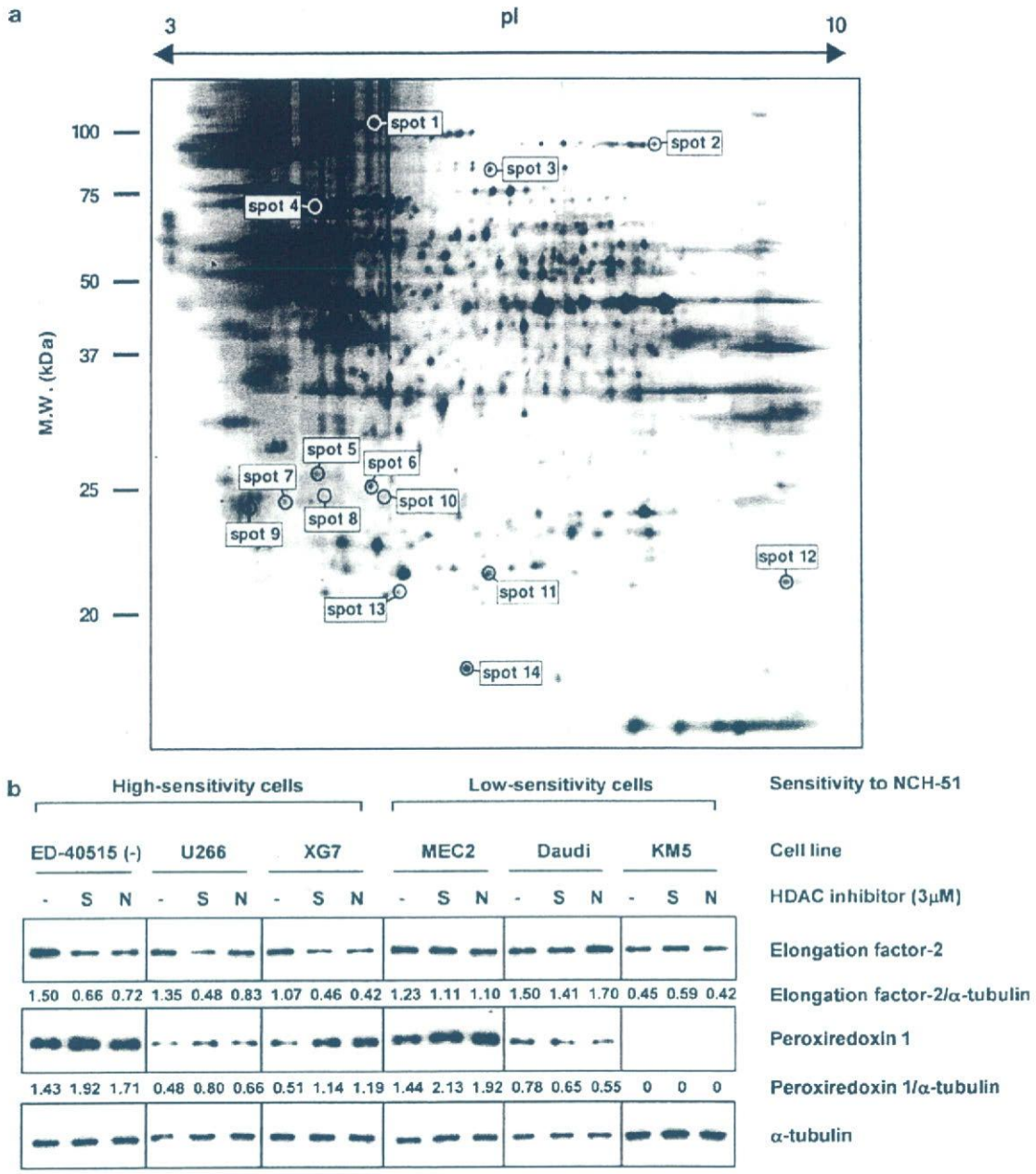

Figure 2 Proteome analysis of the effects of NCH-51. (**a**). 2D electrophoresis image of whole cell proteins prepared from U266 cells. After U266 cells were treated with or without 3 μM NCH-51 for 18 h, the whole cell extracts were prepared and applied to 2D electrophoresis in quadruplicates. Fourteen spots, whose relative amounts were either increased or decreased by the treatment with NCH-51 in all four gels, were indicated. Each spot number in the image corresponds to those in Table 2. MW, molecular weight (kDa). pI, isoelectric point. (**b**) Downregulation of elongation factor-2 (EF-2) and upregulation of peroxiredoxin 1 (PRDX1) by HDACi. The cells were treated with suberoylanilide hydroxamic acid (S) or NCH-51 (N) (3 μM) for 18 h. Whole cell extracts were prepared and subjected to immunoblots with the indicated antibodies. Each value means the ratio of the protein amount to α-tubulin (internal control).

NCH-51 only at the protein level, and PRDX1 and PRDX2 were upregulated primarily at the transcriptional level. These findings suggest that there may be two consequent antioxidative mechanisms by which HDACi modulate ROS accumulation: (i) the mRNA level, acting through induction of transcription of antioxidant molecules *de novo*, and (ii) the protein level, which was presumably caused by blocking the cellular protein transport/degradation pathway involving aggresome and proteasome. Importantly, we have observed that SAHA but not NCH-51 could induce acetylations of α-tubulin and HSP90 (Supplementary Figure 2), suggesting that SAHA might prolong the latter mechanism through blocking the degradation of antioxidant molecules. In fact, SAHA seemed to increase protein expression of PRDX1 greater than NCH-51 (Figure 2b). Since NCH-51 does not retain antioxidant molecules at the protein level, it induces the accumulation of ROS. Cellular levels of antioxidant molecules have been reported to be associated with the sensitivity to conventional anticancer agents.[36] Therefore,

Table 2 Upregulated/downregulated proteins after the treatment with NCH-51 in U266 cells

Spot no.	*Protein ID*	*Protein name*	*MW*	*pI*	*Protein ratio (T/C)*[a]	*mRNA ratio (T/C)*[a]
1	NP_001596	Alanyl-tRNA synthetase (AARS)	106734	5.31	0.80	0.74
2	NP_001952	Elongation factor-2 (EF-2)	95146	6.42	0.82	1.23
3	NP_006830	Mitochondrial inner membrane protein (IMMT)	83626	6.08	0.83	0.64
4	NP_006588	Heat-shock 70 kDa protein 8 (HSPA8)	70854	5.28	0.82	1.18
5	NP_001279	Cl^- intracellular channel protein 1 (CLIC1)	26775	5.09	1.34	0.67
6	NP_002809	Protease activator 28 β subunit (PA28β)	27213	5.44	1.54	1.03
7	NP_004300	Rho GDP-dissociation inhibitor 1 (Rho GDIα)	23193	5.02	1.42	0.92
8	NP_002779	Proteasome subunit α type3	28284	5.19	1.32	0.73
9	NP_663723	14-3-3 ζ/δ (PKC inhibitor protein 1)	28828	4.73	1.37	0.83
10	NP_039234	Cl intracellular channel protein 4 (CLIC4)	28754	5.45	1.38	0.86
11	NP_000843	Glutathione *S*-transferase P 1–1(GSTP1-1)	23210	5.44	1.38	0.98
12	NP_002565	Peroxiredoxin 1 (thioredoxin peroxidase 2) (PRDX1)	22096	8.27	1.30	1.4
13	NP_005800	Peroxiredoxin 2 (thioredoxin peroxidase 1) (PRDX2)	21747	5.67	1.30	1.35
14	NP_000260	Nucleoside disphosphate kinase A (NDPKA)	17138	5.83	1.50	1.04

[a]The results are indicated as the ratio of NCH-51-treated sample to untreated control (T/C).

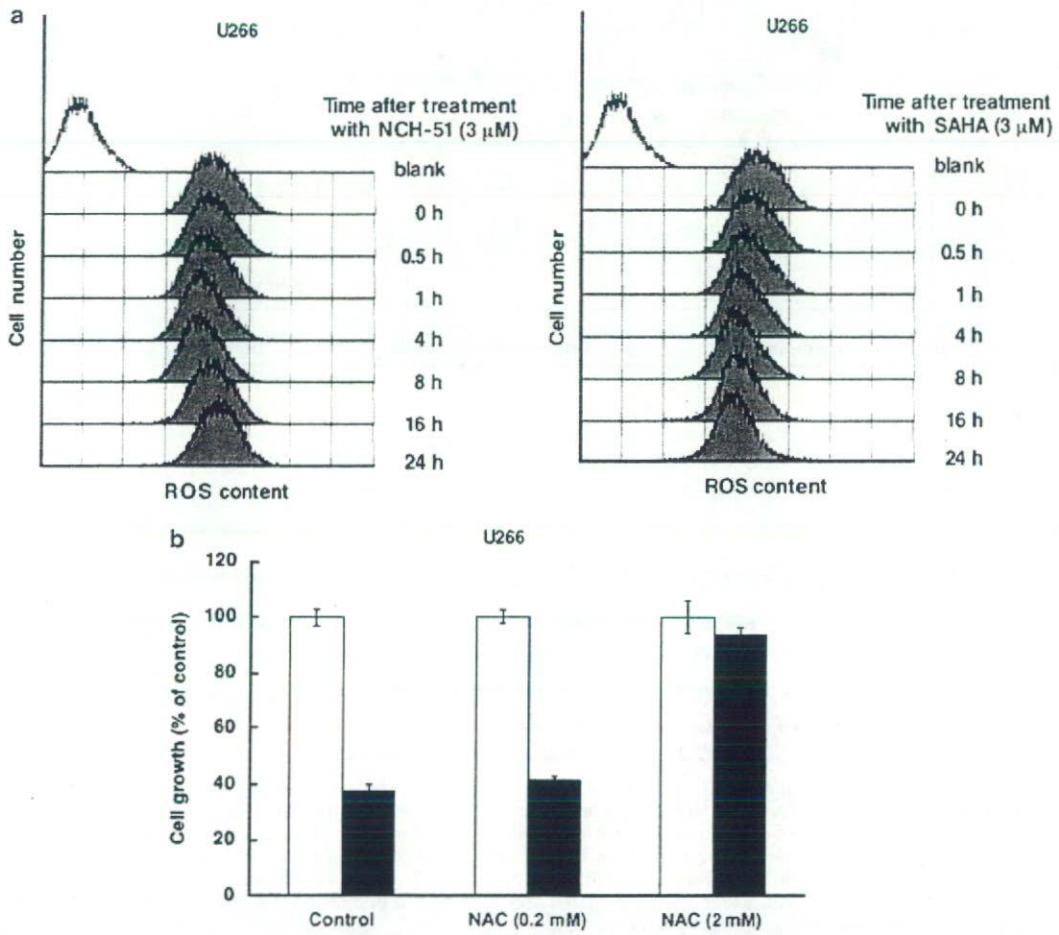

Figure 3 Effects of NCH-51 and suberoylanilide hydroxamic acid (SAHA) on reactive oxygen species (ROS) accumulation. (**a**) Time course of intracellular ROS after the treatment with HDACi. U266 cells were treated with NCH-51 or SAHA (3 μM) given the indicated time (0–24 h). After the treatment, H_2-DCFDA was added and further incubated for 30 min. ROS content was measured by flowcytometry. Blank, H_2-DCFDA-untreated control. (**b**) Effects of *N*-acetyl-L-cysteine (NAC) on the NCH-51-induced cell growth inhibition. U266 cells were treated with or without NCH-51 (3 μM) for 24 h in the presence or absence of NAC (0.2 or 2 mM). Cell growth was measured by 3-(4,5-dimethylthiazol-2-yl)-2,5-diphenyltetrazolium bromide assay. Open and closed bars indicate untreated and the NCH-51-treated cells. The results are shown as the percentage compared to untreated control. Experiments were done in triplicates and the mean values $\pm$s.d. are shown.

NCH-51 can not only induce apoptosis through ROS accumulation, but also enhance the cytotoxicity of other agents in the combination treatment more efficiently than SAHA.

Our proteome analysis has also identified several proteins other than antioxidant molecules, including EF-2, AARS and HSPA8. We confirmed that EF-2 protein, a member of the GTP-

Table 3 ROS content and growth inhibitory effect after the treatment with HDAC inhibitor

Cell line	*ROS content (% of control)*[a]		*Growth inhibition (% of control)*[b]	
	NCH-51 (3 μM)	*SAHA (3 μM)*	*NCH-51 (3 μM)*	*SAHA (3 μM)*
Jurkat	86	47	63.5±0.8	37.7±2.5
MT-2	100	100	38.8±0.3	11.0±2.3
ED-40515 (−)	82	56	71.2±1.2	44.1±1.0
MEC2	59	46	41.3±1.1	3.5±2.8
MO1043	91	65	46.0±0.5	7.2±2.9
Daudi	74	54	25.6±1.8	15.1±3.0
U266	95	85	80.7±1.8	51.7±3.2
XG7	74	28	66.5±1.1	23.1±1.6
KM5	126	119	20.5±0.5	14.6±1.2
ILKM-2	94	94	85.5±0.2	81.3±1.1

Abbreviations: HDAC, histone deacetylase; ROS, reactive oxygen species; SAHA, suberoylanilide hydroxamic acid.
[a]Each value shows the average of 20 000 cells counted.
[b]Each value shows the mean ± s.d.

binding translational elongation factor family,[37] was specifically decreased in high-sensitivity cell lines such as ED-40515 (−) and U266 cells (Figure 2b) after 16 h treatment (data not shown). However, gene expression of EF-2 was upregulated after the treatment with NCH-51 (Table 2). This discrepancy indicates a possibility that NCH-51 could induce rapid turnover of EF-2 protein followed by upregulation of RNA expression. Similar effects on EF-2 were also observed with SAHA (Figure 2b). Since EF-2 has been reported to be inactivated by ROS and lead to inhibition of translation,[38] it is suggested that locally induced ROS by HDACi might induce EF-2 inactivation and degradation presumably by direct oxidation. Although the mechanism by which EF-2 is downregulated by HDACi remains unclear, EF-2 may be used as a feasible surrogate marker to evaluate the susceptibility of HDACi. Similar to EF-2, AARS and HSPA8 were downregulated at the protein level. It is known that HSPA8 are involved in protein folding and transport.[39] Thus, these findings collectively suggest that NCH-51 might arrest protein synthesis and transportation.

In conclusion, our study demonstrates the therapeutic advantage of NCH-51 on growth inhibition of lymphoid malignant cells. Importantly, NCH-51 did not affect the cell growth of normal PBMCs with the effective concentrations on malignant cells (Figure 1b). In addition to its therapeutic efficacy and selectivity, NCH-51 has additional advantages in clinical use based on its pharmacological features. Therefore, NCH-51 could be a useful anticancer agent against lymphoid malignancies.

Acknowledgements

We thank Mr ME Cueno for language editing. This work is supported in part by grant-in-aids from the Ministry of Education, Culture, Sports, Science and Technology and the Ministry of Health, Labor and Welfare of Japan. TS is supported by a grant of Aichi Cancer Research Foundation and a grant of Oujinkai Foundation. HN, TS and NY are supported by a grant of Takeda Science Foundation.

References

1 Minucci S, Pelicci PG. Histone deacetylase inhibitors and the promise of epigenetic (and more) treatments for cancer. *Nat Rev Cancer* 2006; **6**: 38–51.
2 Strahl BD, Allis CD. The language of covalent histone modifications. *Nature* 2000; **403**: 41–45.
3 Turner BM. Cellular memory and the histone code. *Cell* 2002; **111**: 285–291.
4 Claus R, Lubbert M. Epigenetic targets in hematopoietic malignancies. *Oncogene* 2003; **22**: 6489–6496.
5 Fraga MF, Ballestar E, Villar-Garea A, Boix-Chornet M, Espada J, Schotta G *et al.* Loss of acetylation at Lys16 and trimethylation at Lys20 of histone H4 is a common hallmark of human cancer. *Nat Genet* 2005; **37**: 391–400.
6 Seligson DB, Horvath S, Shi T, Yu H, Tze S, Grunstein M *et al.* Global histone modification patterns predict risk of prostate cancer recurrence. *Nature* 2005; **435**: 1262–1266.
7 Kelly WK, Marks PA. Drug insight: histone deacetylase inhibitors–development of the new targeted anticancer agent suberoylanilide hydroxamic acid. *Nat Clin Pract Oncol* 2005; **2**: 150–157.
8 Kelly WK, O'Connor OA, Krug LM, Chiao JH, Heaney M, Curley T *et al.* Phase I study of an oral histone deacetylase inhibitor, suberoylanilide hydroxamic acid, in patients with advanced cancer. *J Clin Oncol* 2005; **23**: 3923–3931.
9 Ryan QC, Headlee D, Acharya M, Sparreboom A, Trepel JB, Ye J *et al.* Phase I and pharmacokinetic study of MS-275, a histone deacetylase inhibitor, in patients with advanced and refractory solid tumors or lymphoma. *J Clin Oncol* 2005; **23**: 3912–3922.
10 Golub LM, Lee HM, Ryan ME, Giannobile WV, Payne J, Sorsa T. Tetracyclines inhibit connective tissue breakdown by multiple non-antimicrobial mechanisms. *Adv Dent Res* 1998; **12**: 12–26.
11 Suzuki T, Nagano Y, Kouketsu A, Matsuura A, Maruyama S, Kurotaki M *et al.* Novel inhibitors of human histone deacetylases: design, synthesis, enzyme inhibition, and cancer cell growth inhibition of SAHA-based non-hydroxamates. *J Med Chem* 2005; **48**: 1019–1032.
12 Huang L, Sowa Y, Sakai T, Pardee AB. Activation of the p21WAF1/CIP1 promoter independent of p53 by the histone deacetylase inhibitor suberoylanilide hydroxamic acid (SAHA) through the Sp1 sites. *Oncogene* 2000; **19**: 5712–5719.
13 Richon VM, Sandhoff TW, Rifkind RA, Marks PA. Histone deacetylase inhibitor selectively induces p21WAF1 expression and gene-associated histone acetylation. *Proc Natl Acad Sci USA* 2000; **97**: 10014–10019.
14 Rosato RR, Almenara JA, Grant S. The histone deacetylase inhibitor MS-275 promotes differentiation or apoptosis in human leukemia cells through a process regulated by generation of reactive oxygen species and induction of p21CIP1/WAF1 1. *Cancer Res* 2003; **63**: 3637–3645.
15 Bali P, Pranpat M, Bradner J, Balasis M, Fiskus W, Guo F *et al.* Inhibition of histone deacetylase 6 acetylates and disrupts the chaperone function of heat shock protein 90: a novel basis for antileukemia activity of histone deacetylase inhibitors. *J Biol Chem* 2005; **280**: 26729–26734.
16 Hubbert C, Guardiola A, Shao R, Kawaguchi Y, Ito A, Nixon A *et al.* HDAC6 is a microtubule-associated deacetylase. *Nature* 2002; **417**: 455–458.

17 Insinga A, Monestiroli S, Ronzoni S, Carbone R, Pearson M, Pruneri G *et al.* Impairment of p53 acetylation, stability and function by an oncogenic transcription factor. *EMBO J* 2004; **23**: 1144–1154.
18 Chen L, Fischle W, Verdin E, Greene WC. Duration of nuclear NF-kappaB action regulated by reversible acetylation. *Science* 2001; **293**: 1653–1657.
19 Hideshima T, Bradner JE, Wong J, Chauhan D, Richardson P, Schreiber SL *et al.* Small-molecule inhibition of proteasome and aggresome function induces synergistic antitumor activity in multiple myeloma. *Proc Natl Acad Sci USA* 2005; **102**: 8567–8572.
20 Sanda T, Asamitsu K, Ogura H, Iida S, Utsunomiya A, Ueda R *et al.* Induction of cell death in adult T-cell leukemia cells by a novel IkappaB kinase inhibitor. *Leukemia* 2006; **20**: 590–598.
21 Uranishi M, Iida S, Sanda T, Ishida T, Tajima E, Ito M *et al.* Multiple myeloma oncogene 1 (MUM1)/interferon regulatory factor 4 (IRF4) upregulates monokine induced by interferon-gamma (MIG) gene expression in B-cell malignancy. *Leukemia* 2005; **19**: 1471–1478.
22 Pulvertaft JV. Cytology of Burkitt's tumour (African lymphoma). *Lancet* 1964; **39**: 238–240.
23 Klein E, Klein G, Nadkarni JS, Nadkarni JJ, Wigzell H, Clifford P. Surface IgM-kappa specificity on a Burkitt lymphoma cell *in vivo* and in derived culture lines. *Cancer Res* 1968; **28**: 1300–1310.
24 Suzuki A, Iida S, Kato-Uranishi M, Tajima E, Zhan F, Hanamura I *et al.* ARK5 is transcriptionally regulated by the Large-MAF family and mediates IGF-1-induced cell invasion in multiple myeloma: ARK5 as a new molecular determinant of malignant multiple myeloma. *Oncogene* 2005; **24**: 6936–6944.
25 Sanda T, Iida S, Ogura H, Asamitsu K, Murata T, Bacon KB *et al.* Growth inhibition of multiple myeloma cells by a novel IkappaB kinase inhibitor. *Clin Cancer Res* 2005; **11**: 1974–1982.
26 Seike M, Kondo T, Mori Y, Gemma A, Kudoh S, Sakamoto M *et al.* Proteomic analysis of intestinal epithelial cells expressing stabilized beta-catenin. *Cancer Res* 2003; **63**: 4641–4647.
27 Imai K, Nakata K, Kawai K, Hamano T, Mei N, Kasai H *et al.* Induction of OGG1 gene expression by HIV-1 Tat. *J Biol Chem* 2005; **280**: 26701–26713.
28 Opferman JT, Korsmeyer SJ. Apoptosis in the development and maintenance of the immune system. *Nat Immunol* 2003; **4**: 410–415.
29 Kawaguchi Y, Kovacs JJ, McLaurin A, Vance JM, Ito A, Yao TP. The deacetylase HDAC6 regulates aggresome formation and cell viability in response to misfolded protein stress. *Cell* 2003; **115**: 727–738.
30 Song EJ, Kim YS, Chung JY, Kim E, Chae SK, Lee KJ. Oxidative modification of nucleoside diphosphate kinase and its identification by matrix-assisted laser desorption/ionization time-of-flight mass spectrometry. *Biochemistry* 2000; **39**: 10090–10097.
31 Arnaud-Dabernat S, Masse K, Smani M, Peuchant E, Landry M, Bourbon PM *et al.* Nm23-M2/NDP kinase B induces endogenous c-myc and nm23-M1/NDP kinase A overexpression in BAF3 cells. Both NDP kinases protect the cells from oxidative stress-induced death. *Exp Cell Res* 2004; **301**: 293–304.
32 Harrop SJ, DeMaere MZ, Fairlie WD, Reztsova T, Valenzuela SM, Mazzanti M *et al.* Crystal structure of a soluble form of the intracellular chloride ion channel CLIC1 (NCC27) at 1.4-A resolution. *J Biol Chem* 2001; **276**: 44993–45000.
33 Shimizu T, Numata T, Okada Y. A role of reactive oxygen species in apoptotic activation of volume-sensitive Cl(−) channel. *Proc Natl Acad Sci USA* 2004; **101**: 6770–6773.
34 Ruefli AA, Ausserlechner MJ, Bernhard D, Sutton VR, Tainton KM, Kofler R *et al.* The histone deacetylase inhibitor and chemotherapeutic agent suberoylanilide hydroxamic acid (SAHA) induces a cell-death pathway characterized by cleavage of Bid and production of reactive oxygen species. *Proc Natl Acad Sci USA* 2001; **98**: 10833–10838.
35 Ungerstedt JS, Sowa Y, Xu WS, Shao Y, Dokmanovic M, Perez G *et al.* Role of thioredoxin in the response of normal and transformed cells to histone deacetylase inhibitors. *Proc Natl Acad Sci USA* 2005; **102**: 673–678.
36 Yokomizo A, Ono M, Nanri H, Makino Y, Ohga T, Wada M *et al.* Cellular levels of thioredoxin associated with drug sensitivity to cisplatin, mitomycin C, doxorubicin, and etoposide. *Cancer Res* 1995; **55**: 4293–4296.
37 Ryazanov AG, Shestakova EA, Natapov PG. Phosphorylation of elongation factor 2 by EF-2 kinase affects rate of translation. *Nature* 1988; **334**: 170–173.
38 Patel J, McLeod LE, Vries RG, Flynn A, Wang X, Proud CG. Cellular stresses profoundly inhibit protein synthesis and modulate the states of phosphorylation of multiple translation factors. *Eur J Biochem* 2002; **269**: 3076–3085.
39 Young JC, Agashe VR, Siegers K, Hartl FU. Pathways of chaperone-mediated protein folding in the cytosol. *Nat Rev Mol Cell Biol* 2004; **5**: 781–791.

Supplementary Information accompanies the paper on the Leukemia website (http://www.nature.com/leu)

Available online at www.sciencedirect.com
ScienceDirect
Mutation Research 619 (2007) 113–123
Fundamental and Molecular Mechanisms of Mutagenesis
www.elsevier.com/locate/molmut
Community address: www.elsevier.com/locate/mutres

Potassium bromate treatment predominantly causes large deletions, but not GC > TA transversion in human cells

Yang Luan [a,b,c], Takayoshi Suzuki [a], Rajaguru Palanisamy [a,d], Yoshio Takashima [b], Hiroko Sakamoto [b], Mayumi Sakuraba [b], Tomoko Koizumi [b], Mika Saito [b,e], Hiroshi Matsufuji [e], Kazuo Yamagata [e], Teruhide Yamaguchi [a], Makoto Hayashi [b], Masamitsu Honma [b,*]

[a] *Division of Cellular and Gene Therapy Products, National Institute of Health Sciences, 1-18-1 Kamiyoga, Setagaya-ku, Tokyo 158-8501, Japan*
[b] *Division of Genetics and Mutagenesis, National Institute of Health Sciences, 1-18-1 Kamiyoga, Setagaya-ku, Tokyo 158-8501, Japan*
[c] *Center for Drug Safety Evaluation, Shanghai Institute of Materia Medica, Chinese Academy of Sciences, 294 Tai-Yuan Road, Shanghai 200031, China*
[d] *Department of Biotechnology, School of Engineering and Technology, Bharathidasan University, Palkalaiperur, Tiruchirappalli 620024, India*
[e] *Department of Food Science and Technology, College of Bioresource Sciences, Nihon University, 1866 Kameino, Fujisawa-shi, Kanagawa 252-8510, Japan*

Received 21 October 2006; received in revised form 24 February 2007; accepted 28 February 2007
Available online 4 March 2007

Abstract

Potassium bromate ($KBrO_3$) is strongly carcinogenic in rodents and mutagenic in bacteria and mammalian cells in vitro. The proposed genotoxic mechanism for $KBrO_3$ is oxidative DNA damage. $KBrO_3$ can generate high yields of 8-hydroxydeoxyguanosine (8OHdG) DNA adducts, which cause GC > TA transversions in cell-free systems. In this study, we investigated the in vitro genotoxicity of $KBrO_3$ in human lymphoblastoid TK6 cells using the comet (COM) assay, the micronucleus (MN) test, and the thymidine kinase (*TK*) gene mutation assay. After a 4 h treatment, the alkaline and neutral COM assay demonstrated that $KBrO_3$ directly yielded DNA damages including DNA double strand breaks (DSBs). $KBrO_3$ also induced MN and *TK* mutations concentration-dependently. At the highest concentration (5 mM), $KBrO_3$ induced MN and *TK* mutation frequencies that were over 30 times the background level. Molecular analysis revealed that 90% of the induced mutations were large deletions that involved loss of heterozygosity (LOH) at the *TK* locus. Ionizing-irradiation exhibited similar mutational spectrum in our system. These results indicate that the major genotoxicity of $KBrO_3$ may be due to DSBs that lead to large deletions rather than to 8OHdG adducts that lead to GC > TA transversions, as is commonly believed. To better understand the genotoxic mechanism of $KBrO_3$, we analyzed gene expression profiles of TK6 cells using Affymetrix Genechip. Some genes involved in stress, apoptosis, and DNA repair were up-regulated by the treatment of $KBrO_3$. However, we could not observe the similarity of gene expression profile in the treatment of $KBrO_3$ to ionizing-irradiation as well as oxidative damage inducers.

Keywords: Potassium bromate ($KBrO_3$); *TK*-mutation; Loss of heterozygosity (LOH); 8-Hydroxydeoxyguanosine (8OHdG); Gene expression profile

* Corresponding author. Tel.: +81 3 3700 1141x435; fax: +81 3 3700 2348.
E-mail address: honma@nihs.go.jp (M. Honma).

0027-5107/$ – see front matter © 2007 Elsevier B.V. All rights reserved.
doi:10.1016/j.mrfmmm.2007.02.029